Journal of Computational Physics 227 (2008) 10243–10262

Contents lists available at ScienceDirect

Journal of Computational Physics

journal homepage: www.elsevier.com/locate/jcp

Parameter estimation in flow through partially saturated porous materials

Kouroush Sadegh Zadeh *

Fischell Department of Bioengineering, University of Maryland, College Park, MD 20742, USA

ARTICLE INFO

Article history:
Received 23 March 2008
Received in revised form 1 September 2008
Accepted 8 September 2008
Available online 16 September 2008

Dedicated to Dr. Hubert J. Montas for his kindness, patience, and sense of humor

MSC:
65R32
74Pxx
76S05
65Mxx
35−xx
74G75
76M20
76B45

Keywords:
Porous media
Inverse modeling
Finite element method
Mass lumping
Richards equation
Levenberg–Marquardt algorithm

ABSTRACT

A class of numerical simulators were developed and critically evaluated to be incorporated as the solver of a forward problem in the framework of an inverse modeling strategy. The strategy couples a mass-lumped Galerkin linear finite element solution of the mixed form Richards equation with an experimental time–space series and the Osborne–Moré revised form of the Levenberg–Marquardt algorithm; to retrieve hydraulic parameters of a partially saturated porous medium. The numerical simulator shows excellent agreement with a *reference solution*, obtained on a dense grid and infinitesimal time step, in terms of fluid pressure head, fluid content, and fluid volumetric flux density and perfectly conserves the global mass. An adaptive algorithm was implemented to estimate sensitivity matrix in the inverse algorithm. A multi-criterion stopping rule was developed and successfully implemented to end the inverse code at the solution. The result of the optimization was compared with a large-scale in-situ soil moisture space–time series, measured during the course of a drainage experiment, and excellent agreements were found. Analysis of the parameter response surfaces and hyper-space plots, closeness of the gradient of the penalty function at minimum to zero, and positive definiteness of the approximation for the Hessian at the solution ($\mathrm{eigs}(H) > 0$) indicate that the obtained solution is a strong local minimum. A state-of-the-art sensitivity analysis carried out to quantify sensitivity of the state variable with respect to uncertainty and changes in different model parameters.

1. Introduction

Despite remarkable efforts to develop state-of-the-art numerical algorithms to solve systems of partial differential equations governing fluid flow and pollutant transport in variably saturated porous media, there have been relatively few attempts to calibrate and validate them against large-scale experimental data sets. The reason is large number of model parameters which requires intensive data sets that are not readily available. The success of these models and corresponding numerical simulators, in describing and understanding the real world and making predictions for them, depends largely on proper representation of relevant processes, uncertainty in model parameters [2], and parameter identification which is a critical step in modeling process [72]. Difficulties in model calibration and parameter identification are quite common in modeling flow and material transport in complex bio-environmental systems. To calibrate these models, one approach is

* Tel.: +1 301 405 0109; fax: +1 301 314 9023.
E-mail address: kouroush@umd.edu.

0021-9991/$ - see front matter © 2008 Elsevier Inc. All rights reserved.
doi:10.1016/j.jcp.2008.09.007

to impose rather restrictive initial and boundary conditions on transport properties of the system that allow direct computation of the parameters. There are several laboratory and large-scale methods to measure the hydraulic and transport parameters in flow and contaminant transport through partially saturated media [9,26]. However, laboratory scale results may not be representative of large scale transport parameters. Large-scale measurements, on the other hand, are tedious, time-consuming, expensive, and often impose unrealistic and simplified initial and boundary conditions on the system. Finally, information regarding parameter uncertainty is not readily obtained from these methods unless a very large number of samples and measurements are taken at significant additional cost [40,72,74,76].

An alternative approach is parameter estimation by inverse modeling. Model calibration, history matching, nonlinear regression, and optimization are equivalent terms for inverse modeling [7,8,15,16,23,29,31,35,43,45–48,50,58,59,64,71,73,77]. Inverse modeling may be viewed as a procedure for converting more easily measured data such as fluid content, fluid pressure head, and concentrations into harder to obtain transport parameters such as kinetic rate constants, hydraulic conductivity of the media, hydrodynamic dispersion coefficient, retardation factor, degradation and production coefficients, and pore water velocity. Unlike direct inversion methods, inverse modeling does not impose any constraints on the form or complexity of the forward model, on the choice of initial and boundary conditions, on the constitutive relationships, or on the treatment of heterogeneities via deterministic or stochastic formulations [76]. Therefore, experimental conditions can be chosen based on convenience rather than by a need to simplify the mathematics of the process. Additionally, if information regarding parameter uncertainty and model accuracy is needed, it can be obtained from the parameter optimization procedure [40,72,76,80].

A general problem in parameter estimation by inverse modeling is ill-posedness [83,72]. Generally, ill-posedness arises from non-uniqueness and instability. Instability occurs when the estimated parameters are excessively sensitive to the input data. Any small errors in measurements will then lead to significant error in estimated values of parameters. If boundary conditions are improperly formulated appreciable errors in parameter optimization may arise. Non-uniqueness occurs when there are multiple parameter vectors that can produce almost the same values of the objective function thus making it impossible to determine the unique solution [81,87,76]. This problem is closely related to parameter identifiability. Parameter identifiability depends on both the structure of the mathematical model and the experimental input data. A common cause for non-identifiability of model parameters is high intercorrelation among parameters. In these situations a change in one parameter generates a corresponding change in the correlated parameter making it impossible to obtain accurate estimate for either of them. Furthermore, even when parameters in a mathematical model are independent of each other, the experimental data may produce an objective function that is not sensitive enough to one or more parameters. The characteristics of the second situation are wide confidence regions on the estimated parameters and large estimation variance. Where a possible solution for the first case is fixing one of the parameters and estimating the other one, in the second case performing multi-objective optimization by coupling different kinds of experimental data may lead to unique solution [40,72].

The goal of this study is to develop, implement, and evaluate an efficient inverse modeling strategy to estimate hydraulic parameters of in partially saturated porous media. A mass-conservative numerical simulator is first developed to solve the initial-boundary value *direct problem* which simulates flow through partially saturated porous media. Neumann boundary conditions are imposed at either ends of the spatial domain. A realistic initial condition in which fluid content of the porous medium varies as a function of the vertical coordinate, is implemented in the numerical simulator and the corresponding physical model to gather the experimental data. To reduce CPU time and maintain small truncation error, an adaptive time-stepping strategy is developed and implemented. The nonlinear matrix equations are solved using the modified Picard iteration scheme. To solve the inverse problem, the Osborne–Moré [54,61] modified version of the Levenberg–Marquardt method [49,52] is used. A switching technique is proposed to calculate the sensitivity matrix (Jacobian matrix) in the inverse code. During each iteration, the algorithm solves the forward problem $p+1$ times (p is number of model parameters being estimated) in the early stages of the optimization by calculating the partial derivatives of the state variable with respect to model parameters by *one-sided finite difference approximation*. As the iteration proceeds and the search approaches the minimum, the algorithm solves the direct problem $2p+1$ times by switching to a *two-sided finite difference scheme* which is more accurate in comparison with the former.

The plan of the paper is as follow: in Section 2 we present a partial differential equation governing fluid flow through partially saturated porous media and the corresponding numerical simulator followed by formulation of the inverse problem in Section 3. Section 4 describes the design of the physical model used to obtain experimental data needed to verify the proposed strategy. Implementation, model verification and calibration, results, and analysis of the developed methodology are also presented in Section 4 followed by concluding remarks in Section 5.

2. Formulation of the forward problem

2.1. Mathematical model

Historically, Richards equation [70], which derives from mass conservation and Darcy–Buckingham law [11,18], has been used to simulate fluid flow in partially saturated porous media:

$$\frac{\partial\theta}{\partial t}-\frac{\partial}{\partial z}\left[K(h)\left(\frac{\partial h}{\partial z}-1\right)\right]=0 \tag{1}$$

where θ is the volumetric fluid content of the medium (L^3L^{-3}), h is fluid pressure head (L), $K(h)$ is unsaturated hydraulic conductivity function (LT^{-1}), z is vertical spatial dimension (L^{-1}), assumed positive downward, and t is time (T).

Solution of (1) requires constitutive relations among fluid pressure, fluid content of the porous medium (saturation), and hydraulic conductivity [73]. A common form of the fluid pressure–saturation relationships, which was used in this study, is van Genuchten's expression [86]:

$$\theta = \theta_r + (\theta_s - \theta_r)[1 + (\alpha_v h)^{n_v}]^{-m_v} \tag{2}$$

in which θ_s is the saturated fluid content (L^3L^{-3}), θ_r is residual fluid content (L^3L^{-3}), α_v is air entry value (L^{-1}), and n_v and $m_v = 1 - 1/n_v$ are curve fitting parameters.

The pressure head–hydraulic conductivity relation was described using Mualem's model [56]:

$$K(h) = \frac{K_s(1 - (\alpha_v h)^{n_v m_v}[1 + (\alpha_v h)^{n_v}]^{-m_v})^2}{[1 + (\alpha_v h)^{n_v}]^{lm_v}} \tag{3}$$

where K_s is the saturated hydraulic conductivity of the medium (LT^{-1}) and l is pore connectivity index.

The proposed algorithm, to solve Eq. (1), is not dependent on the precise form of the constitutive relations. The algorithm was tested against a wide variety of closed form constitutive relationships including the Brooks and Corey–Burdine [10,12], Brooks and Corey–Mualem [86], van Genuchten–Burdine [85], Kossugi [41,42], and Assouline [3,4] expressions. The results are only reported for Mualem–van Genuchten model [56,85].

2.2. Discretization

Due to the highly nonlinear nature of Richards equation, its solution is not possible analytically unless unrealistic and over-simplifying assumptions are made. Therefore, numerical solutions are usually the only viable procedures to treat flow and transport phenomena in partially saturated porous media. To develop a finite element approximation of (1), the flow domain was first divided into a series of finite linear elements which join one another in nodal points. The weak formulation of the state variables and the constitutive relations were then approximated using interpolating polynomials [33,36,67,90]. It is assumed that the hydraulic conductivity varies linearly within each element [72]:

$$h(z,t) \simeq \hat{h}(z,t) = \sum_{j=1}^{N} h_j(t)\phi_j(z) \tag{4}$$

$$\theta(h,t) \simeq \hat{\theta}(h,t) = \sum_{j=1}^{N} \theta_j(h)\phi_j(z) \tag{5}$$

$$K^{n+1,m} \simeq \widehat{K} = \sum_{j=1}^{N} K_j^{n+1,m}\phi_j(z) \tag{6}$$

in which i represents location in the finite element mesh and n and m denote time step and iteration level, respectively, N is total number of nodes, $\phi_j(z)$ are piecewise linear basis functions, and $h_j(t)$ are the associated time-dependent unknown coefficients representing solutions of (1) at nodal points within the domain. Note that $K(h)$ is estimated in new time step but previous iteration level.

Substituting (4)–(6) into (1) will not satisfy the partial differential equation and hence will produce an error or residual. The goal of the finite element approximation is to minimize this error. Based on the weighted residual principle, which is becoming standard approach to treat fluid flow and mass transport processes in partially saturated porous media, the error minimization can be accomplished by introducing the weight function, $\phi_i(z)$, and setting the integral of the weighted residuals to zero. Note that the finite element approximation can also be based on the variational principle which minimizes a physical quantity over the entire domain and leads to algebraic equations [89]. However, this approach is not applicable to any differential equation containing a first derivative (see [79] for a lucid discussion on the disadvantages of the variational method and advantages of Galerkin's approach):

$$\int_0^L \left[\frac{\partial\hat{\theta}}{\partial t} - \frac{\partial}{\partial z}\left[\widehat{K}(h)\left(\frac{\partial\hat{h}}{\partial z} - 1\right)\right]\right]\phi_i(z)\mathrm{d}z = 0 \qquad i = 1,2\ldots,N \tag{7}$$

where L is the length of the spatial domain.

Performing integration by parts (Green's theorem) to reduce the second derivative and inserting (4)–(6) into (7) yields:

$$\int_0^L \frac{\partial\left(\sum_{j=1}^{N}\theta_j(t)\phi_j(z)\right)}{\partial t}\phi_i(z)\mathrm{d}z + \sum_{j=1}^{N} h_j \int_0^L K\frac{\partial\phi_i(z)}{\partial z}\frac{\partial\phi_j(z)}{\partial z}\mathrm{d}z + \int_0^L \frac{\partial K}{\partial z}\phi_i(z)\mathrm{d}z = 0 \quad i = 1,2,\ldots,N \tag{8}$$

In Galerkin's method, which was used in this study, the weight functions are chosen to be identical to the basis function [72].

The time derivative in (8) was discretized by a fully implicit finite difference scheme. Expanding the fluid content of the porous medium at new time step and iteration level with respect to h about the expansion point $h_i^{n+1,m}$ by Taylor series expansion [14]:

$$\theta^{n+1,m+1} = \theta^{n+1,m} + \left.\frac{\mathrm{d}\theta}{\mathrm{d}h}\right|^{n+1,m} (h^{n+1,m+1} - h^{n+1,m}) + \cdots \tag{9}$$

and ignoring the higher order terms, substituting the truncated series into (8), evaluating the integrals, and assembling the global matrices; the matrix form of the finite element approximation of (1) can be developed as

$$\begin{aligned}
&\left[\left(C_{i-1}^{n+1,m} + C_i^{n+1,m}\right)\frac{\Delta z}{12\Delta t} + \frac{K_{i-1}^{n+1,m} + K_i^{n+1,m}}{2\Delta z}\right] h_{i-1}^{n+1,m+1} \\
&+ \left[\left(C_{i-1}^{n+1,m} + 6C_i^{n+1,m} + C_{i+1}^{n+1,m}\right)\frac{\Delta z}{12\Delta t} + \frac{K_{i-1}^{n+1,m} + 2K_i^{n+1,m} + K_{i+1}^{n+1,m}}{2\Delta z}\right] h_i^{n+1,m+1} \\
&+ \left[\left(C_i^{n+1,m} + C_{i+1}^{n+1,m}\right)\frac{\Delta z}{12\Delta t} + \frac{K_{i+1}^{n+1,m} + K_i^{n+1,m}}{2\Delta z}\right] h_{i+1}^{n+1,m+1} \\
&= \left[\left(C_{i-1}^{n+1,m} + C_i^{n+1,m}\right)\frac{\Delta z}{12\Delta t}\right] h_{i-1}^{n+1,m} + \left[\left(C_{i-1}^{n+1,m} + 6C_i^{n+1,m} + C_{i+1}^{n+1,m}\right)\frac{\Delta z}{12\Delta t}\right] h_i^{n+1,m} + \left[\left(C_i^{n+1,m} + C_{i+1}^{n,m}\right)\frac{\Delta z}{12\Delta t}\right] h_{i+1}^{n+1,m} \\
&\quad + \left(\theta_{i-1}^{n} + 4\theta_i^{n} + \theta_{i+1}^{n}\right)\frac{\Delta z}{6\Delta t} - \left(\theta_{i-1}^{n+1,m} + 4\theta_i^{n+1,m} + \theta_{i+1}^{n+1,m}\right)\frac{\Delta z}{6\Delta t} - \frac{K_{i+1}^{n+1,m} - K_{i-1}^{n+1,m}}{2}
\end{aligned} \tag{10}$$

where

$$C^{n+1,m} = \left.\frac{\mathrm{d}\theta}{\mathrm{d}h}\right|^{n+1,m} \simeq \widehat{C}^{n+1,m} = \sum_{j=1}^{N} C_j^{n+1,m}\phi_j(z) \tag{11}$$

is the soil water capacity function or capacitance term (L^{-1}). It is assumed that C varies linearly within each element [72]. Similar to $K(h)$, the capacitance term was estimated in new time step but previous iteration level.

2.3. Mass lumping

To increase efficiency of (10) and prevent possible oscillatory behavior and convergence problems, the *mass lumping* approach was used [57,84]. Mass lumping was performed by defining the nodal values of the time derivative as weighted averages over the entire flow region:

$$\int_0^L C\frac{\partial h}{\partial t}\phi_i(z)\mathrm{d}z \approx \frac{\partial h_i}{\partial t}\int_0^L C\phi_i(z)\mathrm{d}z, \quad i = 1, 2\ldots, N \tag{12}$$

which produces:

$$\begin{aligned}
&\left[\frac{K_{i-1}^{n+1,m} + K_i^{n+1,m}}{2\Delta z}\right] h_{i-1}^{n+1,m+1} + \left[\left(C_{i-1}^{n+1,m} + 4C_i^{n+1,m} + C_{i+1}^{n+1,m}\right)\frac{\Delta z}{6\Delta t} + \frac{K_{i-1}^{n+1,m} + 2K_i^{n+1,m} + K_{i+1}^{n+1,m}}{2\Delta z}\right] h_i^{n+1,m+1} + \left[\frac{K_{i+1}^{n+1,m} + K_i^{n+1,m}}{2\Delta z}\right] h_{i+1}^{n+1,m+1} \\
&= \left[\left(C_{i-1}^{n+1,m} + 4C_i^{n+1,m} + C_{i+1}^{n+1,m}\right)\frac{\Delta z}{6\Delta t}\right] h_i^{n+1,m} + \left(\theta_{i-1}^{n} + 4\theta_i^{n} + \theta_{i+1}^{n}\right)\frac{\Delta z}{6\Delta t} - \left(\theta_{i-1}^{n+1,m} + 4\theta_i^{n+1,m} + \theta_{i+1}^{n+1,m}\right)\frac{\Delta z}{6\Delta t} - \frac{K_{i+1}^{n+1,m} - K_{i-1}^{n+1,m}}{2}
\end{aligned} \tag{13}$$

Comparing this equation with (10), shows that the diagonal elements of the *lumped stiffness mass matrix* are identical to the row sums of the entries of the distributed matrix. The linear finite element may be further simplified by redefining the lumped mass matrix to yield:

$$\begin{aligned}
&\left[\frac{K_{i-1}^{n+1,m} + K_i^{n+1,m}}{2\Delta z}\right] h_{i-1}^{n+1,m+1} + \left[\frac{\Delta z}{\Delta t}C_i^{n+1,m} + \frac{K_{i-1}^{n+1,m} + 2K_i^{n+1,m} + K_{i+1}^{n+1,m}}{2\Delta z}\right] h_i^{n+1,m+1} + \left[\frac{K_i^{n+1,m} + K_{i+1}^{n+1,m}}{2\Delta z}\right] h_{i+1}^{n+1,m+1} \\
&= \frac{\Delta z}{\Delta t}C_i^{n+1,m} h_i^{n+1,m} + \left(\theta_{i-1}^{n} + 4\theta_i^{n} + \theta_{i+1}^{n}\right)\frac{\Delta z}{6\Delta t} - \left(\theta_{i-1}^{n+1,m} + 4\theta_i^{n+1,m} + \theta_{i+1}^{n+1,m}\right)\frac{\Delta z}{6\Delta t} - \frac{K_{i+1}^{n+1,m} - K_{i-1}^{n+1,m}}{2}
\end{aligned} \tag{14}$$

2.4. Implementation of initial and boundary conditions

The initial and boundary conditions applied to the discrete domain were selected to represent the experimental conditions described in Section 4.1. To solve (1), a zero flux boundary condition ($\frac{\mathrm{d}h}{\mathrm{d}z} = 1$) was applied at the top and a free drainage boundary condition ($q = K$, where q is the volumetric fluid density flux (LT^{-1})) was applied at the bottom of the spatial

domain. Initial soil water contents were measured before the initiation of the drainage experiment and as Fig. 1 shows these initial data vary as a function of vertical coordinate (depth). A quadratic function was fitted to these measurements:

$$\theta(z,0) = -2.9133 \times 10^{-6} z^2 + 5.9528 \times 10^{-4} z + 0.4069 \tag{15}$$

and used, through Eq. (2), to set the initial condition for the forward problem.

2.5. Iterative procedure and adaptive time-stepping

The system of algebraic equations produced by numerical solution of (1) are nonlinear because of the dependence of the hydraulic functions $K(h)$ and $C(h)$ upon the solution. In this study, a linearization–iteration approach was used to solve the partial differential equation (Note that there are nonlinear ordinary differential equations techniques such as the *method of lines* [82] to solve (1) which is beyond the scope of this study). The iteration methods that are generally used are the Picard and Newton algorithms. Theoretically, Newton's method converges one order of magnitude faster than the Picard scheme [19], but several studies have shown that this method is inferior to the Picard method [44,65,66]. Newton's method converges quadratically only in the vicinity of the solution. When the estimated values are far from the solution the method produces severe non-physical oscillation in the iteration process and diverges. This is a consequence of the neglected higher order terms in the Taylor series expansion, which contribute to the right hand side vector of the system of linear equations and are still significant, leading to a Jacobian matrix devoid of diagonal dominance. In contrast, the Picard method produces a symmetrical and diagonally dominant matrix. Furthermore, evaluation of the Jacobian matrix in Newton's method is often time consuming especially for highly nonlinear partial differential equations such as Richards. Because of these issues, the Modified Picard algorithm was selected. In this approach, the hydraulic functions are calculated using pressure head at the current time but previous iteration level ($h_i^{n+1,m}$). The system of algebraic equations is solved for pressure head with these approximate values of $K(h)$ and $C(h)$. The updated pressure head values are then compared to those of the previous iteration. When the maximum difference between the new and previous pressure head values is less than the convergence criterion the iteration stops and the system is solved for the next time step. A small nonzero value for soil water capacity function at or near saturation was also applied ($C \geqslant \delta$) where δ is the threshold value of the capacitance term [73].

To decrease CPU time and maintain acceptable truncation error an adaptive time-stepping approach was used. As implemented in the numerical simulator of the forward problem, the time step starts with a prescribed initial time increment; then the time increment is increased by 5% if the number of Picard iterations for the previous time step was less than δ_1 and it is decreased by five per cent if the number of Picard iterations was greater than δ_2 (δ_1 and δ_2 are user defined integers; $\delta_1 < \delta_2$).

2.6. Global mass balance

An accurate numerical simulator should conserve the global mass over the entire spatio-temporal domain. Global mass conservation is a necessity but not sufficient condition for the acceptability of a numerical solver. In this study, the mass balance was calculated by [14]:

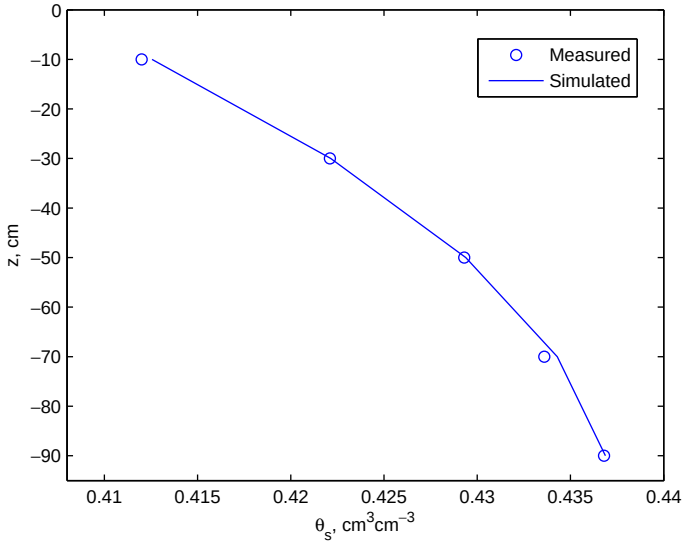

Fig. 1. Measured and predicted initial volumetric soil moisture content as a function of soil depth.

$$\mathrm{MB}(t)=\frac{\sum_{i=1}^{N-1}(\theta_i^{n+1}-\theta_i^0)\Delta z+(\theta_0^{n+1}-\theta_0^0)\frac{\Delta z}{2}+(\theta_N^{n+1}-\theta_N^0)\frac{\Delta z}{2}}{\int_0^t K_{N-1/2}[\frac{(h_N-h_{N-1})}{\Delta z}-1]\mathrm{d}\tau-\int_0^t K_{1/2}\left[\frac{(h_1-h_0)}{\Delta z}-1\right]\mathrm{d}\tau} \tag{16}$$

The expressions in the denominator are nodal fluid density fluxes at the upper ($i=1$) and lower ($i=N$) boundaries of the spatial domain calculated using Darcy–Buckingham law [11,18,32].

3. Formulation of the inverse problem

The inverse problem was treated as a nonlinear optimization problem in which model parameters were estimated by minimizing an appropriate objective function, $\phi(p)$, representing the discrepancy between the measured and predicted state variables [5,6,78]:

$$\phi(p)=\frac{1}{2}\sum_{i=1}^{N} r_i(p)^2 \tag{17}$$

where r is the residual column vector (differences between the measured and predicted fluid contents), N is number of observations, and $p=[K_s,\alpha_v,n_v,\theta_r,l]$ is the parameter vector being optimized.

3.1. Optimization algorithm

Different Newton-based optimization algorithms were tested to minimize (17). While evaluation of the *Hessian* in Newton's method, which is not available analytically, was ineffectively time-consuming; the Gauss–Newton scheme showed rank-deficiency and the *steepest descent* method was too inefficient requiring a large number of iterations. Although this behavior of the method is well known for non-convex functions such as Rosenbrock's valley or banana function [5], some investigators have recently used it to parameterize flow and pollutant transport in groundwater systems [38,39]. The standard Levenberg–Marquardt algorithm [49,52] was also tested where it was fast but exhibited singularity and oscillatory behavior (nevertheless, this method was recently used by Malengier [51]) to retrieve flow parameters in a drainage problem). Finally using QR decomposition [25], the linear least square problem below which is the Osborne–Moré [54,61] adaptation of the Levenberg–Marquardt algorithm:

$$\left\|\begin{pmatrix} r(p^k)\\ 0\end{pmatrix}+\begin{pmatrix} J(p^k)\\ (\lambda^k D^k)^{1/2}\end{pmatrix}\Delta p^k\right\|^2 \tag{18}$$

was solved to obtain search direction (step direction), Δp^k, in each iteration of the inverse algorithm:

$$\begin{pmatrix} J(p^k)\\ (\lambda^k)^{1/2}D^k\end{pmatrix}\Delta p^k=-\begin{pmatrix} r(p^k)\\ 0\end{pmatrix} \tag{19}$$

in which $D=\mathrm{diags}(d_1,d_2,\ldots,d_p)$ is a positive definite scaling symmetric matrix which assures the descent property of the algorithm, λ is the Lagrange multiplier which controls both the magnitude and direction of Δp^k, k is iteration level in the inverse algorithm, and J is the $N\times p$ Jacobian or sensitivity matrix:

$$J=\frac{\partial r_i(p)}{\partial p_i}=-\frac{\partial h(p)}{\partial p_i} \tag{20}$$

where h was obtained by (14). Since the derivatives of h with respect to model parameters are not available analytically, a combination of *one-sided* and *two-sided* finite difference method was implemented to calculate the partial derivatives of the state variable (h) with respect to model parameters. At the early stages of the optimization, where the search is far from the minimum, the *one-sided finite difference scheme*, which is computationally cheap, was used [72]:

$$J=-\frac{U(p_1,\ldots,p_i+\delta p_i,\ldots,p_n)-U(p_1,\ldots,p_i,\ldots,p_n)}{\delta p_i} \tag{21}$$

As the optimization proceeds in descent direction the algorithm switches to a more accurate but computationally expensive approach in which the partial derivatives are calculated using a *central finite difference scheme* [72]:

$$J=-\frac{U(p_1,\ldots p_i+\delta p_i,\ldots,p_n)-U(p_1\ldots,p_i-\delta p_i,\ldots,p_n)}{2\delta p_i} \tag{22}$$

The switch was made when $\phi(p)\leqslant\delta$, where δ is user defined small value.

Given that λ is a positive scalar, the approximation of the Hessian matrix must be positive definite in order to insure the descent property of the algorithm. To achieve this, the value of D was initialized using a $p\times p$ identity matrix before the optimization loop. By implementing the algorithm below in the inverse code, the diagonal elements were updated in each iteration [77]:

for $i = 1 : p$ **do**
$D(i,i) = \max(\|J(:,i)\|, D(i,i))$
end for

In order to update λ in each iteration, the optimization starts with an initial parameter vector and a large λ. As long as the objective function decreases in each iteration, the value of λ is reduced. Otherwise, it is increased. The approach avoids calculation of λ and step length in each iteration and therefore is computationally cheap [76].

3.2. Termination criterium

One of the most crucial steps in nonlinear optimization is an effective stopping criterion. The criterium should insure converges, to a global or strong local minimum (or maximum in case of maximization), with the least possible iterations. The rules below were implemented in the inverse code and critically evaluated to select and implement the most effective termination criterium:

1. The first stopping rule was based on the changes in the parameter values at each iteration:
   if $\Delta p \leqslant \delta_1$ **then**
   Stop
   else
   Continue optimization
   end if
   where δ_1 is user defined small value.Numerical test problem showed that a stopping rule based on the changes in the parameter values at each iteration is not effective. In some cases the parameters do not change significantly over several iterations, then they change suddenly and produce significant reduction in the magnitude of the penalty function. Therefore, this termination rule is not recommended for nonlinear optimization.
2. Another criterion was the relative and absolute changes in the magnitude of the penalty function at each iteration:
   if $\frac{\Delta\phi(p^{k+1})}{\phi(p^k)} \leqslant \delta_2$ & $\Delta\phi(p^k) \leqslant \delta_3$ **then**
   Stop
   else
   Continue optimization
   end if
   In which δ_2 and δ_3 are user defined small values.Our experience indicates that stopping rule based on the absolute and relative changes in the magnitude of the objective function in every iteration is case dependent. For small values of δ_2 and δ_3 the algorithm runs repeatedly without significant changes in the penalty function. For large values of δ_2 and δ_3 the solution may not be satisfactory. Therefore, a judicious choice of δ_2 and δ_3 is operational and depends on the knowledge and expertise of the user.
3. A third termination criterium, which was tested, was the norm of the gradient of the objective function at solution ($\|\nabla\phi(p = \hat{p})\|$):
   if $\|\nabla\phi(p = \hat{p})\| \leqslant \delta_4$ **then**
   Stop
   else
   Continue optimization
   end if
   where δ_4 is user defined small value and $\hat{p}$ is the optimized parameter vector at the solution.Although the true measure of the closeness of the solution to a real minimum is the norm of the gradient of the objective function at the solution (which should be zero), in our experience $\|\nabla\phi_i p = \hat{p})\|$ seldom converges to zero yet the solution is quite satisfactory (see Table 1 and Fig. 5). A large number of algorithm runs are required to obtain small changes in $\phi(p)$ without significant changes in the values of the model parameters.

Finally, critically evaluating these rules, a multi-rule termination criterium was implemented in the inverse code to stop the iteration process at the solution:

if $\|\nabla\phi(p = \hat{p})\| \leqslant \delta_5$ & $\Delta p \leqslant \delta_2$ & $\frac{\Delta\phi(p^{k+1})}{\phi(p^k)} \leqslant \delta_3$ & $\Delta\phi(p^k) \leqslant \delta_4$ **then**
Stop
else
Continue optimization
end if

The termination criterium was found to be effective (see Fig. 6).

Table 1
The results of parameter estimation for drainage experiment

p[a]	$\hat{p}$	$LL_{0.95}$	$UL_{0.95}$	$\nabla\phi(p)$	σ_p^2	$\frac{\sigma_p^2}{p}$	$\left\|\frac{\partial\theta}{\partial p}\right\|$
K_s	5.9388	5.0009	6.8767	0.0000	0.2204	0.0371	0.0406
α_v	0.0308	0.0257	0.0359	−0.0002	0.0001	0.0032	8.4122
n_v	1.4429	1.3661	1.5197	0.0000	0.0015	0.0010	1.8203
θ_r	0.0000	–	–	0.0001	0.0018	0.0018	1.2739
l	−4.6735	−6.7135	−2.6335	0.0000	1.0428	0.2231	0.0316

[a] The units for K_s and α_v are cm d^{-1} and cm^{-1}, respectively, while other parameters are dimensionless. $LL_{0.95}$ and $UL_{0.95}$ are the 95% lower limit and upper limit confidence intervals on the optimized values of parameters. $\nabla\phi(p)$ is the gradient of the penalty function at the solution, σ_p^2 is parameter's variance, $\frac{\sigma_p^2}{p}$ is parameter's relative variance, and $\|\frac{\partial\theta}{\partial p}\|$ is the norm of the parameter's relative sensitivity.

4. Implementation and results

4.1. Physical model

To evaluate the applicability and efficacy of the developed forward and inverse algorithms in estimation of model parameters in real world, a $2 \times 2 \times 1.25$ m^3 lysimeter with layered soil was equipped with five time domain reflectometry (TDR) probes (three 20 cm rods of 0.3 cm diameter and with 2.5 cm separation) to monitor spatio-temporal distribution of soil water contents during the course of one month drainage experiment. The probes were inserted horizontally at depths 10, 30, 50, 70, and 90 cm. They were multiplexed and connected to a TRASE TDR device (Soilmoisture Inc., Santa Barbara, CA). The lysimeter was saturated by providing ponding water at the top of the soil profile and allowing free drainage at the bottom for two weeks. Then, the drain tube was blocked and the surface of the lysimeter was covered by nylon, providing a zero flux Neumann boundary condition at the top of the spatial domain. After two weeks, free drainage was initiated by unblocking the drain pipe and was continued over one month. This provides a free drainage Neumann boundary condition at the lower end of the spatial domain. The soil moisture content was measured at five different depths frequently. Fig. 2 shows schematic representation of the physical model.

The resulting time–space series was coupled with the numerical simulator and the developed inverse modeling strategy to estimate the hydraulic parameters of the soil.

4.2. Validation of the numerical simulator

Before being incorporated into the framework of the developed inverse modeling strategy, the numerical model should be *validated* against an exact solution ([60] presents an excellent review article on the validation, verification, and confirmation of numerical models). Since it is essentially impossible to obtain an analytic solution for Eq. (1) without imposing over-simplifying assumptions about the soil water characteristic relationship, the numerical simulator was validated against a

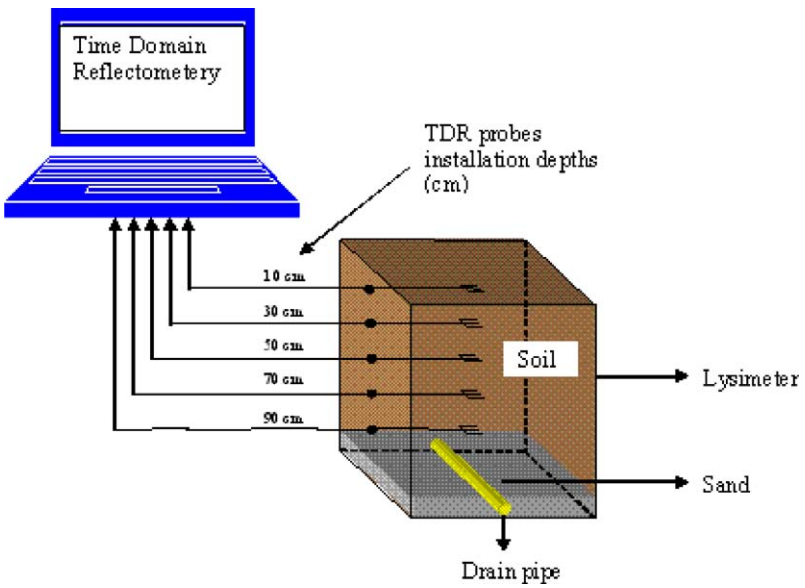

Fig. 2. Schematic representation of the physical model.

reference solution using a numerical test problem. The test problem was a drainage experiment with a zero flux boundary condition at the top of the domain and a free drainage Neumann boundary condition at the bottom. The soil water hydraulic parameters were taken from Sadegh Zadeh [72] and are as follows: $K_s = 12.5$ cm d^{-1}, $\alpha_v = 0.014$ cm^{-1}, $n_v = 1.5$, $\theta_r = 0.05$, $\theta_s = 0.33$, and $l = 0.5$. The experiment was simulated by Eq. (14) for a dense grid with a very fine time step ($\Delta z = 0.1$ cm and $\Delta t = 1 \times 10^{-9}$ day), which was used to represent the *reference solution*. The numerical simulator was then used to reproduce the drainage experiment using a coarse grid and large time interval typical of values used during optimization ($\Delta z = 2.50$ cm and $\Delta t = 1 \times 10^{-2}$ day).

Fig. 3 presents the results of model validation in terms of spatial and temporal distributions of soil water pressure head (3(a)) and soil water content (3(b)). The figure indicates that in the early stages of the simulation there are discrepancies between the solver and the *reference solution*. The reason for discrepancy is steep gradient in fluid pressure head at the beginning of the drainage. To eliminate the deviation, small time increment was used. Furthermore, to promote robustness of the simulator two time indices were implemented in the adaptive time-stepping loop. In any time step if the time increment became less than Δt_{min} it was set to Δt_{min} (since Δt_{min} produces excellent fit and reasonable global mass balance, there is no need to use $\Delta t < \Delta t_{min}$ as well as $\Delta t > \Delta t_{max}$) and if the time interval became more than Δt_{max} it was set to Δt_{max}. The time increment cannot exceed these two limits ($\Delta t_{min} < \Delta t < \Delta t_{max}$), where Δt_{min} and Δt_{max} are user defined scalars. To control time increment, the following time-stepping algorithm was implemented at the end of the Picard loop (inside the time loop):

if Picard iteration counter < 4 **then**
  $\Delta t = 1.05 \times \Delta t$
else if Picard iteration counter < 7 **then**
  $\Delta t = \Delta t$

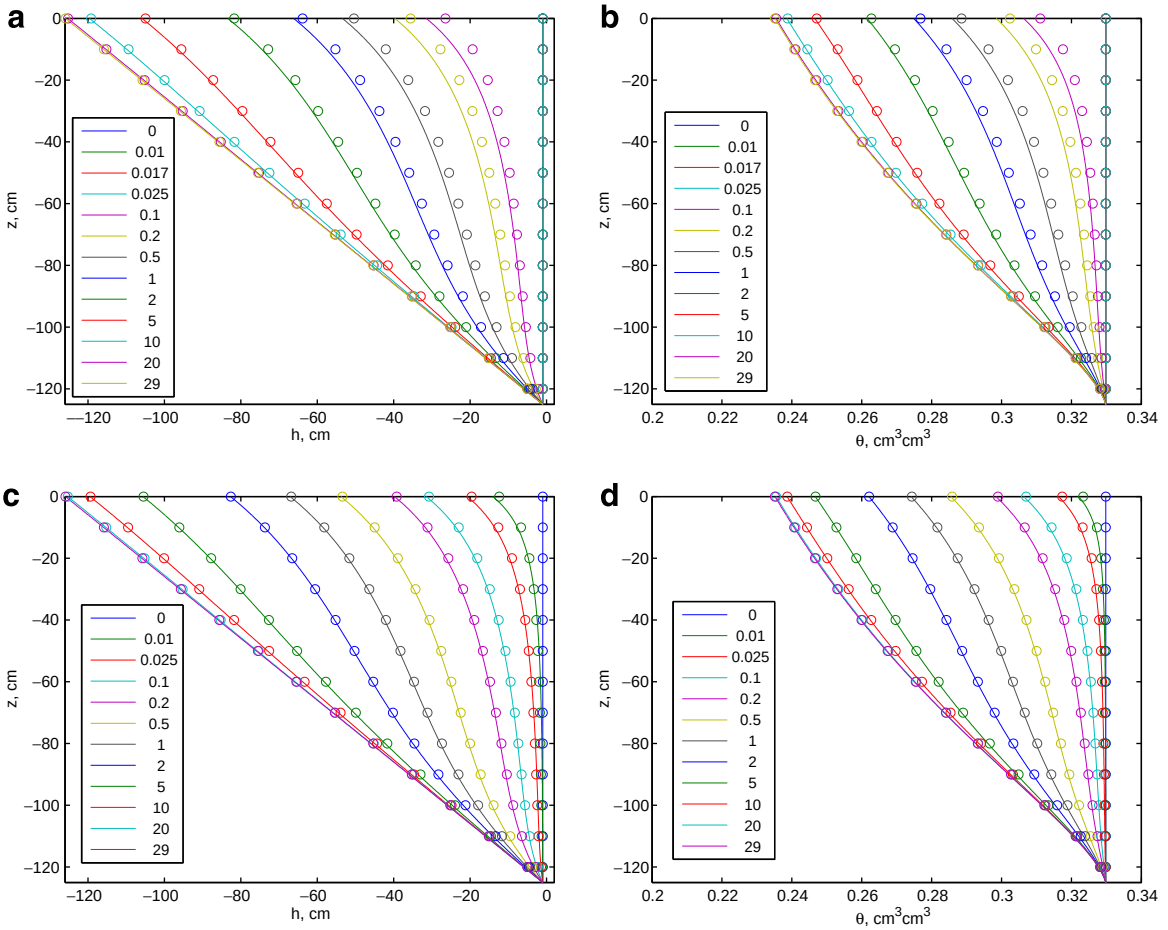

Fig. 3. Spatial and temporal distributions of soil water pressure head (a and c) and soil water content (b and d) during the course of a one-month drainage experiment, generated by the mass-lumped Galerkin linear finite element solution of the direct problem (dots) and the *reference solution* (solid lines). Figures (c) and (d) were produced using the revised time-stepping loop ($\Delta t_{min} < \Delta t < \Delta t_{max}$). The legend indicates the times after initiation of free drainage (in days).

else
$\Delta t = 0.95 \times \Delta t$
end if
if $\Delta t < \Delta t_{\min}$ **then**
$\Delta t = \Delta t_{\min}$
else if $\Delta t > \Delta t_{\max}$ **then**
$\Delta t = \Delta t_{\max}$
end if

The results of the revised time-stepping loop were depicted in Fig. 3(c) (for soil water pressure head profile) and d (for soil water content profile). Furthermore, the mass-lumped Galerkin linear finite element solution of the mixed form Richards equation was compared with the reference solution, in terms of cumulative outflow, in Fig. 4(a). The cumulative outflow was calculated by Darcy–Buckingham law [11,18,32] at the last node as a function of drainage time:

$$q_N^{n+1} = -K_{N-1/2}^{n+1}\left[\frac{h_N^{n+1} - h_{N-1}^{n+1}}{\Delta z} - 1\right] \tag{23}$$

Fig. 3(c), (d) and 4(a) indicate that the numerical simulator shows excellent agreement with the reference solution in modeling fluid pressure head and fluid content profiles as well as cumulative outflow during the course of a drainage experiment.

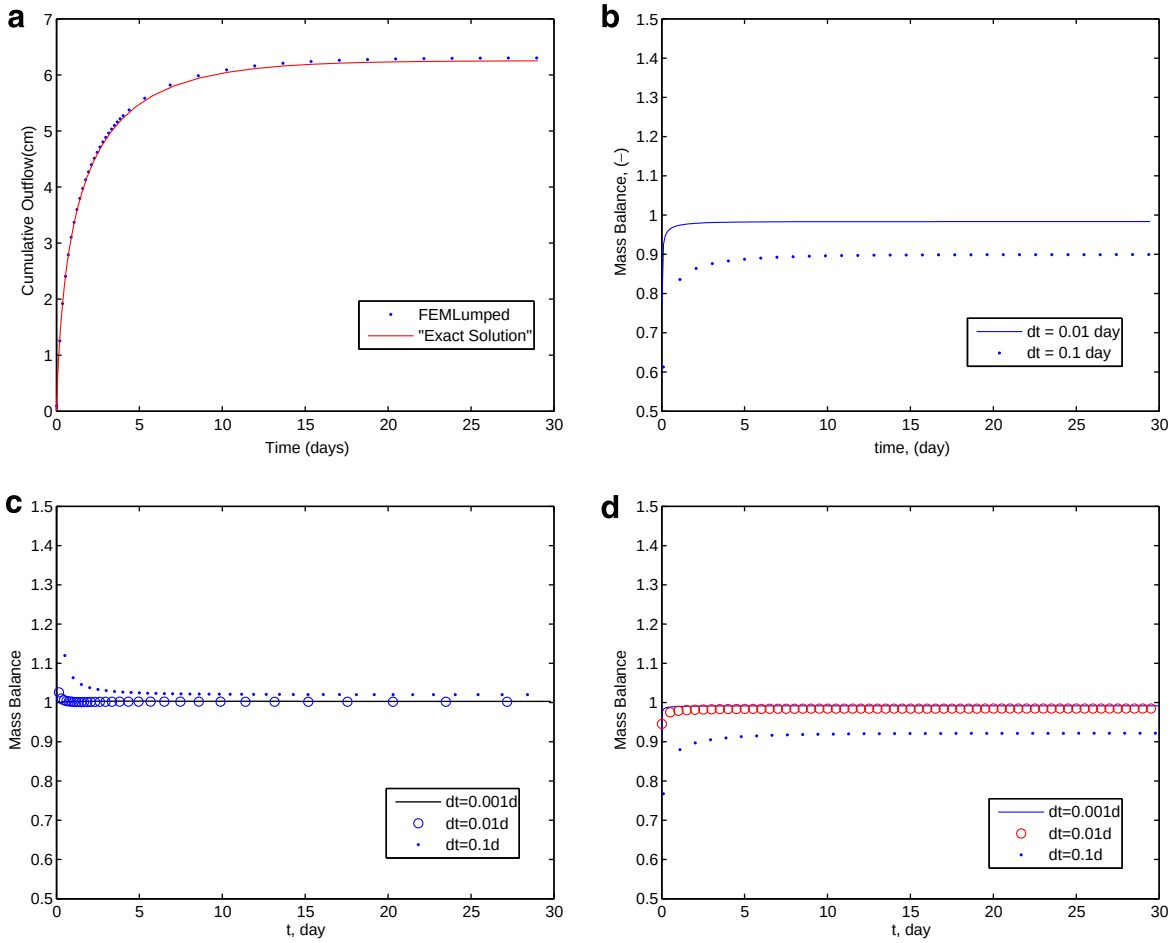

Fig. 4. (a) Comparison of the mass-lumped Galerkin linear finite element solution of the mixed form Richards equation with the *reference solution* in terms of cumulative outflow calculated by Darcy–Buckingham law. (b) Mass conservation property of the mixed form Richards equation with *distributed stiffness mass matrix* (i.e., Eq. (10)) using different initial time increments, (c) Global mass balance error of the h-based form Richards equation with *mass-lumped matrix* using different initial time steps, and (d) Mass conservation property of the proposed numerical simulator for different time steps.

4.3. Mass conservation property of the simulator

The global mass balance error of the numerical simulators is presented in Fig. 4(b)–(d). Fig. 4(b) shows mass conservation property of the solver with *distributed stiffness mass matrix*, Eq. (10), for different initial time steps. The simulator shows poor mass balance for $\Delta z = 2.50$ cm and $\Delta t = 1 \times 10^{-1}$ day. The error is about 40% at the beginning of the simulation when the gradient is steep and changes in the soil water pressure head is high. It reaches 10% as the simulation proceeds. The distributed mass matrix also showed oscillatory behavior and had convergence problem. The simulator did not converge or the rate of convergence was painfully slow in modeling infiltration of water into dry soils (results not shown) which is in contrast with the results observed by Huyakoran et al. [34]. However, the simulator, as Fig. 4(b) shows, produces acceptable mass balance error for $\Delta z = 2.50$ cm and $\Delta t = 1 \times 10^{-2}$ day for drainage problem (not for infiltration into dry soil).

The global mass conservation property of the mass-lumped Galerkin linear finite element solution of the *h-based form* Richards equation is presented in Fig. 4(c) for sake of comparison. The error is more pronounced for $\Delta z = 2.50$ cm and $\Delta t = 1 \times 10^{-1}$ day so that it reaches 30% at the beginning of the drainage experiment. However, the simulator shows excellent mass balance for $\Delta z = 2.50$ cm and $\Delta t = 1 \times 10^{-2}$ day and specifically for $\Delta z = 2.50$ cm and $\Delta t = 1 \times 10^{-3}$ day over entire domain and for all times. Again, the finite element solver of the *h-based form* Richards equation suffers from sever mass balance error when used to model infiltration into dry soils (results not shown). This behavior of the formulation has been well documented in the porous media community [14,20,24,30,37,53,62,63,75].

Finally, the mass balance property of Eq. (14) is depicted in Fig. 4(d). The simulator conserves global mass with near perfection for $\Delta z = 2.50$ cm and $\Delta t = 1 \times 10^{-2}$ day as well as for $\Delta z = 2.50$ cm and $\Delta t = 1 \times 10^{-3}$ day. Note that for $\Delta t = 1 \times 10^{-2}$ the maximum mass balance error is less than 5%. The simulator, however, shows poor mass balance for $\Delta t = 1 \times 10^{-1}$ day especially at the beginning of the simulation. This is in contrast with the findings of Celia et al. [14] who reported that numerical solvers (both finite element and finite difference though finite difference is superior) of the mixed form Richards equation is mass-conservative for any time steps and any boundary conditions.

In conclusion, the distributed mass matrix linear finite element solver of the *mixed form Richards equation* (Eq. (10)) as well the *mass-lumped* linear finite element solver of the *h-based form Richards equation* produced poor mass balance and therefore were not selected as the simulator of the forward problem to be incorporated into the inverse strategy developed in this study. The Crank–Nicolson scheme [17] was also tested for both the finite element and finite difference approximations. For similar mesh, the scheme was unstable and the rate of convergence was inefficiently slow particularly for infiltration into very dry soils. Therefore, the proposed inverse strategy couples Eq. (14), as simulator, with the experimental time–space series and Eq. (19) to retrieve hydraulic parameters in flow through variably saturated porous media.

5. Hydraulic parameter estimation

In order to retrieve model parameters $p = [K_s, \alpha_v, n_v, \theta_r, l]$, the penalty function (17) was minimized iteratively by first starting with an initial guess of parameter values and updating it in each iteration until the termination criterium was met:

$$p^{(k+1)} = p^{(k)} + \alpha^{(k)} \Delta p^{(k)} \tag{24}$$

where $\alpha^{(k)}$ is step length [5].

The results of optimization are presented in Fig. 5 and Table 1. Fig. 5 demonstrates that the developed inverse modeling strategy can be successfully used to identify hydraulic parameters of partially saturated porous media. The coefficients of determinations (R^2) for depths of 10, 30, 50, 70, and 90 cm are 0.9918, 0.9919, 0.9905, 0.9868, and 0.9750, respectively. The overall coefficient of determination is $R^2 = 0.9908$ which implies that the forward model can explain more than 99% of the temporal and spatial soil water content distribution during the time course of a drainage experiment. The root mean squared error (RMSE) was found to be 0.0045 which is very low. The coefficient of determination and the root mean squared error were calculated by [72]

$$R^2 = \frac{\left[\sum_{i=1}^{N} \hat{\theta}_i \theta_i - \sum_{i=1}^{N} \hat{\theta}_i \sum_{i=1}^{N} \theta_i\right]^2}{\left[\sum_{i=1}^{N} \hat{\theta}_i^2 - \left(\sum_{i=1}^{N} \hat{\theta}_i\right)^2\right]\left[\sum_{i=1}^{N} \theta_i^2 - (\sum \theta_i)^2\right]} \tag{25}$$

$$\mathrm{RMSE} = \sqrt{\frac{r^T r}{N - p}} \tag{26}$$

where θ_i and $\hat{\theta}_i$ are the observed and predicted soil water content, respectively.

The efficacy of the proposed inverse algorithm, especially the multi-rule stopping criterium, is depicted in Fig. 6. The figure presents evolution of the penalty function as a function of iteration level in the inverse algorithm. The initial guess for optimization was: $K_s = 10$ cm d^{-1}, $\alpha_v = 0.05$ cm^{-1}, $n_v = 1.2$, $\theta_r = 0.05$, and $l = 0.5$. The optimized parameter values are given in the first column of Table 1. Notice that it is user's responsibility to provide meaningful initial guess for the parameter vector. The following constraints (regularization) were employed in this study: $K_s > 0$ cm d^{-1}, $\alpha_v > 0$ cm^{-1}, $n_v > 1$, $\theta_r > 0$. The pore connectivity index was kept variable.

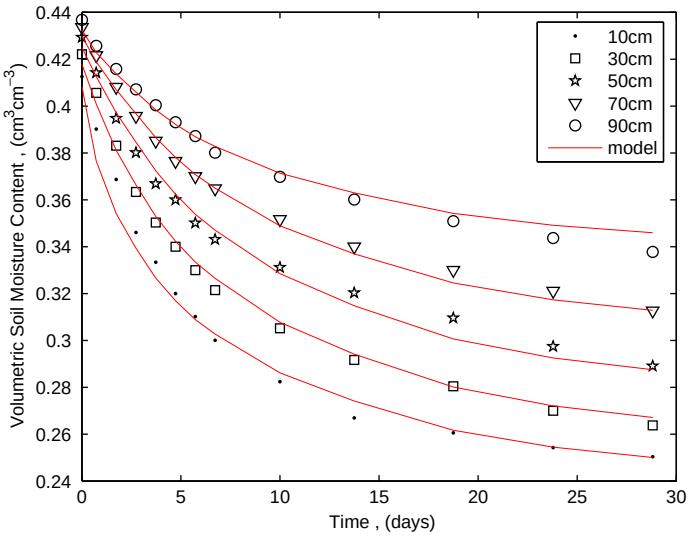

Fig. 5. Spatial and temporal distribution of the observed and simulated soil water contents during drainage experiment. The legend shows the measurement depths in centimeter.

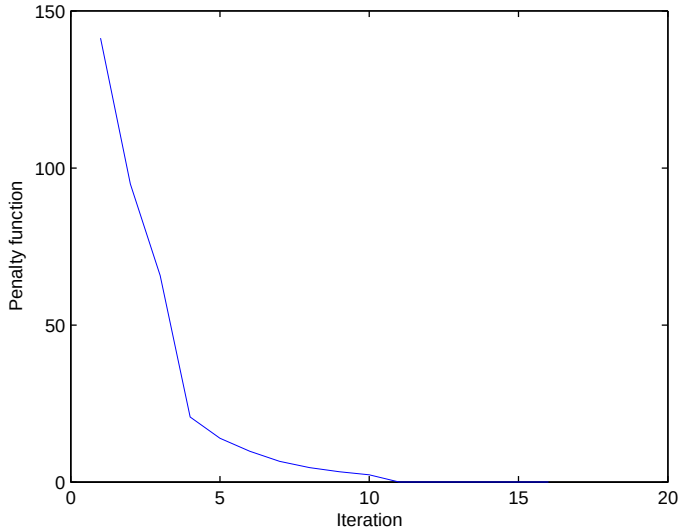

Fig. 6. Evolution of the penalty function as a function of iteration level in the inverse algorithm developed. The initial guess for optimization was: $K_s = 10\ \mathrm{cm\ d^{-1}}, \alpha_v = 0.05\ \mathrm{cm^{-1}}, n_v = 1.2, \theta_r = 0.05$, and $l = 0.5$. The optimized parameter values are given in the first column of Table 1.

5.1. Statistical assessment of the inverse problem

One of the advantages of the inverse modeling over the commonly used model calibration is uncertainty analysis which can be accomplished at the end of the parameter optimization procedure. The second-order approximation of the *parameter covariance matrix* was obtained by [72]:

$$C = s^2 (H)^{-1} \tag{27}$$

where H is the Hessian matrix and s is the estimated error variance:

$$s = \frac{r^T r}{N - p} \tag{28}$$

The diagonal elements of the parameter covariance matrix are variances which indicate parameter estimation uncertainty and the off-diagonal elements are covariances between the parameters. Using this matrix one can calculate the *parameter correlation* or *variance–covariance* matrix which is a square matrix [5,72]:

$$V = \frac{C_{ij}}{\sqrt{C_{ii}}\sqrt{C_{jj}}} \tag{29}$$

Eq. (29) identifies the degree of correlation between the optimized parameters. In other words, the correlation matrix quantifies the nonorthogonality between two parameters. A value of ± 1 reflects perfect linear correlation between two parameters whereas 0 suggests no linear correlation at all. The matrix may be used to identify which parameter, if any, is better kept constant in the parameter optimization process [86].

The confidence intervals on the optimized parameters were calculated using parameter covariance matrix [72]:

$$pr\left(\hat{p} - t\sqrt{C_{ii}} \leqslant \hat{p} \leqslant \hat{p} + t\sqrt{C_{ii}}\right) = \gamma \tag{30}$$

where C_{ii} is the parameter variances, obtained by the covariance matrix, and $t \equiv t_{v,1-\alpha/2}$ is the value of the *Student's t distribution* [1] for confidence level $\gamma = 1 - \alpha$ and degree of freedom v (α is level of significance).

Note that these equations are taken from linear regression and hold only approximately for nonlinear optimization. Furthermore, to use these equations $\hat{p}$ should be the true minimum and no constraints should be imposed on the parameter space. Under these conditions, Eqs. (27)–(30) show reasonable agreement with the nonlinear optimization statistics [21].

Table 1 presents the optimized values of the hydraulic parameters, the 95% confidence intervals on the parameters, the gradient of the objective function at the solution, the variances of the parameter estimation, the relative parameter estimation variance $\left(\frac{\sigma_p^2}{p}\right)$, and the norm of the parameter sensitivity $\left(\left\|\frac{\partial\theta}{\partial p}\right\|\right)$. Since the gradient of the objective function at the solution is almost zero and the *approximation for the Hessian* is positive definite (eigs(H) = [0.0000 0.0001 0.0332 0.5400 85.5013]), the solution is at least a strong local minimum. Except for the pore connectivity index (l), the estimation variance and confidence intervals of the optimized values of the parameters indicate that the hydraulic parameters can be identified with more accuracy and small residual errors using the inverse strategy developed. Since the estimated value of the residual water content is zero, confidence intervals were not reported for this parameter (in the inverse code the value of θ_r is set to zero if θ_r becomes less than 0.005).

Although the pore connectivity index (l) was estimated by Mualem [55] to be 0.5 as an average for about 50 different soil types, his catalogue consisted mainly of packed soils, many of them being relatively coarse-textured. The commonly used $l = 0.5$ may produce reasonable results for repacked and sandy soils, but it may not be suitable for medium- and, especially, fine-textured soils as was shown in this study. There are several other research works reporting similar findings. van Genuchten [86] reports that l ranges between -5 and +5. Our results further suggest that the pore connectivity index should be estimated by parameter optimization techniques as it will likely improve fitting process. However, notice that the confidence intervals for this parameter are relatively wide indicating poor identifiability of this parameter through drainage experiment. Note also that the optimized parameter values show excellent agreements with the parameter response surface plots which will be discussed in Section 5.2.

5.2. Analysis of the parameter response surface

The uniqueness of the inverse problem was investigated by construction of the parameter response surface plots. Response surfaces are two-dimensional plots of the objective function and are useful in providing information about the linearity of the model and possibility of multiple minima or maxima [72]. Ten pairs of response surface plots were constructed for parameter vector $p = [K_s, \alpha_v, n_v, \theta_r, l]$ and depicted in Figs. 7 and 8. The domain of each parameter was discretized into 50 discrete points resulting in 2500 grid points for each response surface implying that the direct problem should be solved 25,000 times to generate ten plots.

The $K_s - \alpha_v$ and $K_s - n_v$ planes in Figs. 7(a) and (b) show well-defined valleys which start at small value of K_s and large values of α_v and n_v and extend in hyperbolic shape in K_s-direction. The response surfaces show an inverse relationship between K_s and α_v as well as K_s and n_v in terms of their effects on the objective function. An increase in K_s in higher subspace of the parameter domain and corresponding decrease in α_v and n_v in lower subspace produce the same behavior in the objective function, $\phi(\theta)$.

Analysis of the hyperbolic shape of $\phi(\theta)$ in Fig. 7(a) suggests that for higher values of α_v (lower values of K_s) the objective function becomes insensitive to α_v, but in lower subspace of α_v (higher values of K_s) it becomes insensitive to K_s. In the middle part of the parameter space, both parameters are more identifiable. The hyperbolic behavior of the penalty function $\phi(\theta)$ in Fig. 7(b) indicates that K_s is more identifiable in the middle part of the domain of n_v. It also suggests that n_v is more identifiable in the relatively small subspace of K_s. The objective function becomes insensitive to K_s in lower values of n_v (higher values of K_s) and actually extends parallel to K_s-direction. On the other hand, $\phi(\theta)$ becomes insensitive to n_v in lower values of K_s and higher values of n_v. The plot in this region is almost parallel to n_v.

Fig. 7(c) presents the response surface plot of the objective function in $\alpha_v - n_v$-direction. Again, the response surfaces show an inverse relationship between α_v and n_v in terms of their effects on the penalty function. An increase in α_v in higher subspace of the parameter domain and corresponding decrease in n_v in lower subspace causes the same response in $\phi(\theta)$. The hyperbolic shape of $\phi(\theta)$ suggests that for higher values of α_v (lower values of n_v) the objective function becomes insensitive to α_v, but in lower subspace of α_v (higher values of n_v) it becomes insensitive to n_v. In the middle part of the plot both parameters are more identifiable. Note that there are an infinite combinations of parameters α_v and n_v around the *error level*

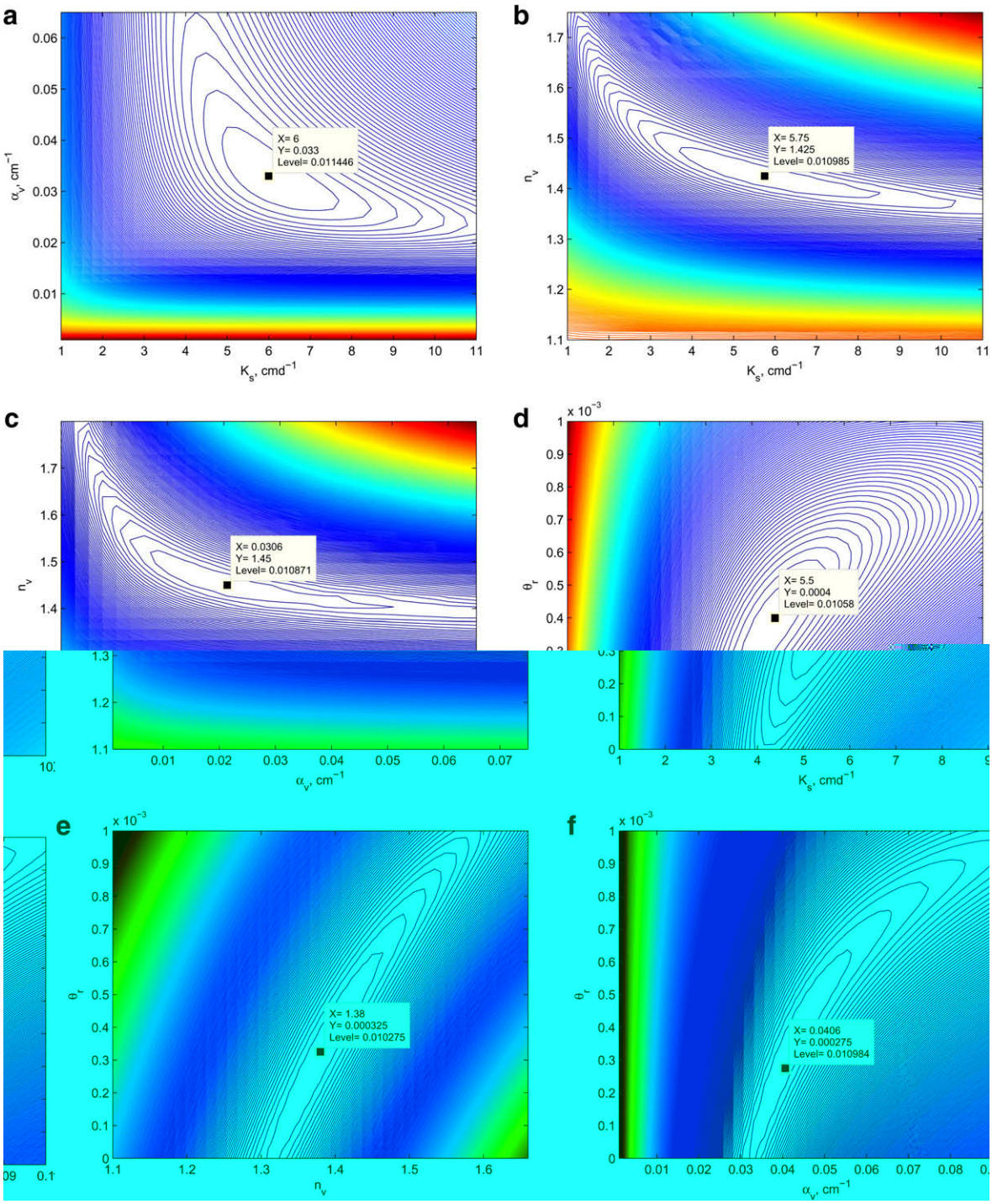

Fig. 7. Contours of the penalty function in $K_s - \alpha_v$ (a), $K_s - n_v$ (b), $\alpha_v - n_v$ (c), $K_s - \theta_r$ (d), $n_v - \theta_r$ (e), and $\alpha_v - \theta_r$ (f) planes. The magnitude of the penalty function at minimum is given by *level*.

(denoted as *level* in the plot) that can produce almost $\phi(\theta) = 0.01$. This indicates that the bottom of the objective function at the vicinity of the solution is very flat and it is very difficult or essentially impossible to obtain unique values for α_v and n_v simultaneously (see [73] for a lucid discussion on the problems of simultaneous estimation of α_v and n_v).

Figs. 7(d) show the response surface plot of the objective function in the $K_s - \theta_r$ plane. The plot shows a well-defined minimum. K_s and θ_r in all of the response surfaces converged to $\simeq 6$ cm d^{-1} and zero, respectively, which are their optimized values obtained through inverse modeling. In other words, the inverse modeling and the response surfaces produced the

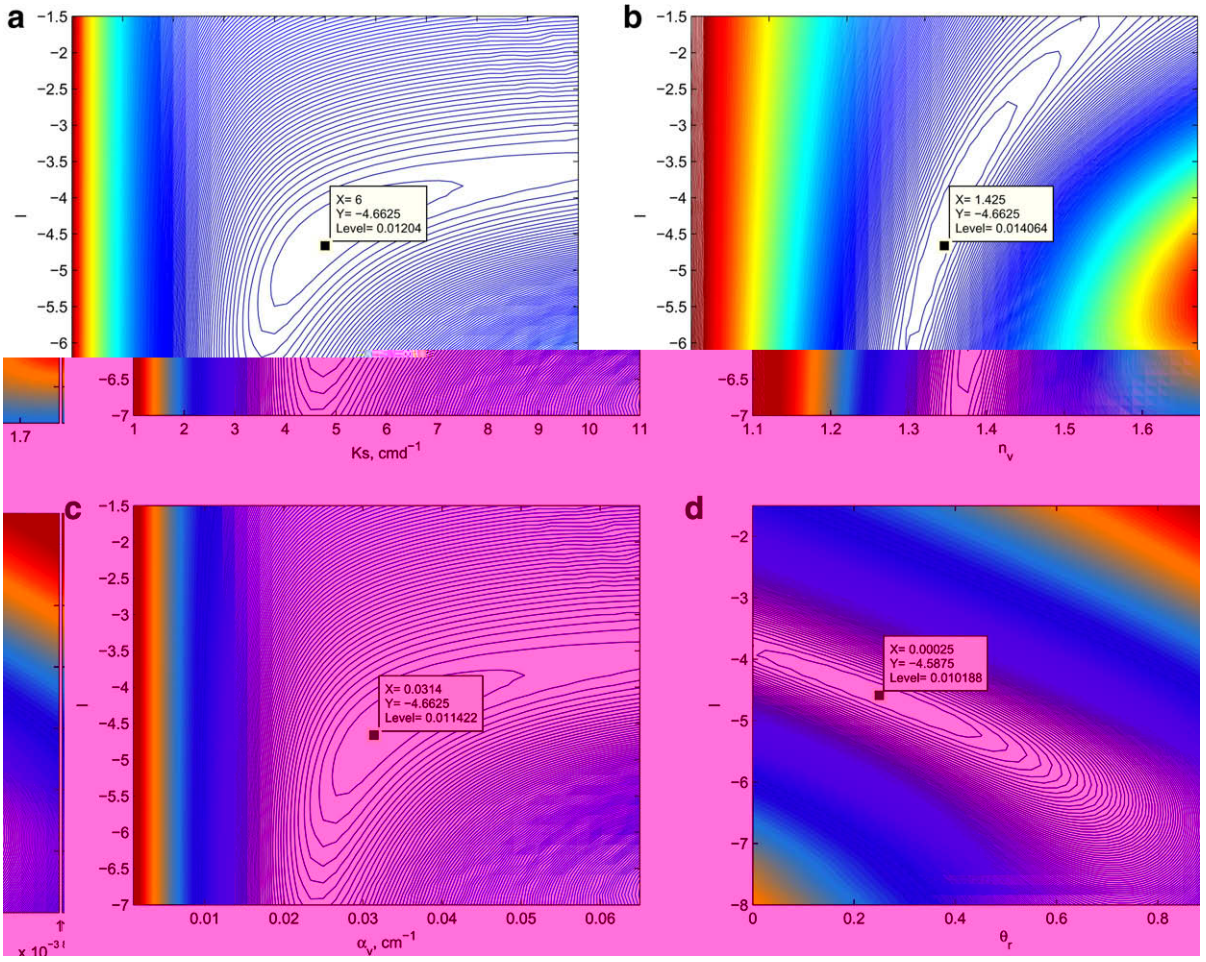

Fig. 8. Contours of the penalty function in $K_s - l$ (a), $n_v - l$ (b), $\alpha_v - l$ (c), and $\theta_r - l$ (d) planes. The magnitude of the penalty function at minimum is given by *level*.

same values for saturated hydraulic conductivity and residual water content. Figs. 7(e) and (f) show the response surface plots of the objective function in the $n_v - \theta_r$ and $\alpha_v - \theta_r$ planes. The objective function has a very well-defined minimum in Fig. 7(d)–(f). In other words, the soil water content data produces useful information to identify θ_r. This is expected since the residual soil water content, by definition, is the water content at -1500 kPa soil water pressure head and should be better estimated by the soil moisture data in the dry region of soil moisture characteristics curve.

Contours of the objective function in $l - K_s, l - n_v, l - \alpha_v$ and $l - \theta_r$ planes are presented in Fig. 8(a)–(d), respectively. The planes show well-defined minimum in all of the plots. The planes in Figs. 8(a)–(c) plots start at low values of the parameters and extend in logarithmic shape through almost the entire parameter space. In lower subspace of the parameters the response surfaces are almost parallel to l. In the middle of the plots there are direct relationships between l, in one hand, and other three parameters, on the hand, in terms of their effects on the penalty function (in the middle part of the parameter domain parameters are more identifiable and the objective function produces a well-defined minimum). In large values of the parameters, however, $\phi(\theta)$ approaches its minimum value and becomes almost constant. Indeed, in higher values of K_s, n_v, and α_v the contours of penalty function become parallel to these parameters making it impossible to obtain unique values for them. Fig. 8(d) presents the response surface plot of $\phi(\theta)$ in the $l - \theta_r$ plane. The pore connectivity index ($l = -4.6735$) was found to be far different than the value of $l = 0.50$ which has been extensively used in the unsaturated flow modeling [13,14,40,56,86]. One may conclude that the objective function is insensitive to l since the pore connectivity index varies from -6.7135 to -2.6335. These inferences are consistent with the results of Table 1 in which the parameter confidence interval for l is wider than other parameters and the estimation variance for this parameter $\left(\frac{\sigma_l^2}{l} = 0.2231\right)$ is the highest among the optimized hydraulic parameters. Note that the norm of the sensitivity of the model with respect to the changes in l is the least ($\left\|\frac{\partial\theta}{\partial l}\right\| = 0.0316$) among the parameters (see Table 1).

In conclusion, the minimum in all response surface plots converge the same parameter values obtained by the optimization algorithm. Note also that the magnitude of the penalty function in all plots is almost the same ($\phi(p = \hat{p}) = 0.01$) and coincides with the value obtained by the nonlinear optimization (see Fig. 6).

5.3. Parameter hyper-space

Since response surface plots are only two-dimensional cross sections of a whole parameter domain, analysis of the behavior of the penalty function in full hyper-space will reveal how the function might behave in the whole space. To fully understand the behavior of the objective function, $\phi(\theta)$, in whole parameter space a five-dimensional hyper-space should be constructed and demonstrated which is not technically plausible in foreseeable future. However, to gain broader perspective on the identifiability of the model parameters through inverse modeling, three-dimensional parameter hyper-spaces were constructed and analyzed. Domain of each parameter was discretized into 100 discrete points resulting in one million grid points for the target hyper-space. This requires solving the forward problem, Eq. (14), one million times which takes about one week run of a Pentium4 Processor 550 (3.4 GHz) PC for each hyper-space plot. Four of the generated plots are presented in Fig. 9 for $K_s - n_v - l$ (a), $l - K_s - \theta_r$ (b), $l - n_v - \theta_r$ (c), and $K_s - n_v - \theta_r$ (d) patches. The logarithm of the penalty function at the solution is given in the legend.

The plots show distinct minimum patch. Note the elongated patch in l-direction which is consistent with the response surface plots and high estimation variance and broad confidence intervals on this parameter in Table 1.

5.4. Sensitivity analysis

Sensitivity analysis quantifies sensitivity of models to variation or uncertainty in model parameters. It is a key technique to determine the dependence of a system's behavior on the parameters that could possibly affect the dynamics of the system. If a small change in a parameter yields relatively large changes in the state variable(s), model, and/or system; the outcomes are said to be sensitive to that parameter. These kinds of parameters are good control points of the system dynamics and should be determined accurately to achieve a reliable outcome. Parameters to which model behavior exhibits minor sensitivity do not require laborious measurements. These Parameters are likely not good control points of the system behavior [22,27,28,68,69,88].

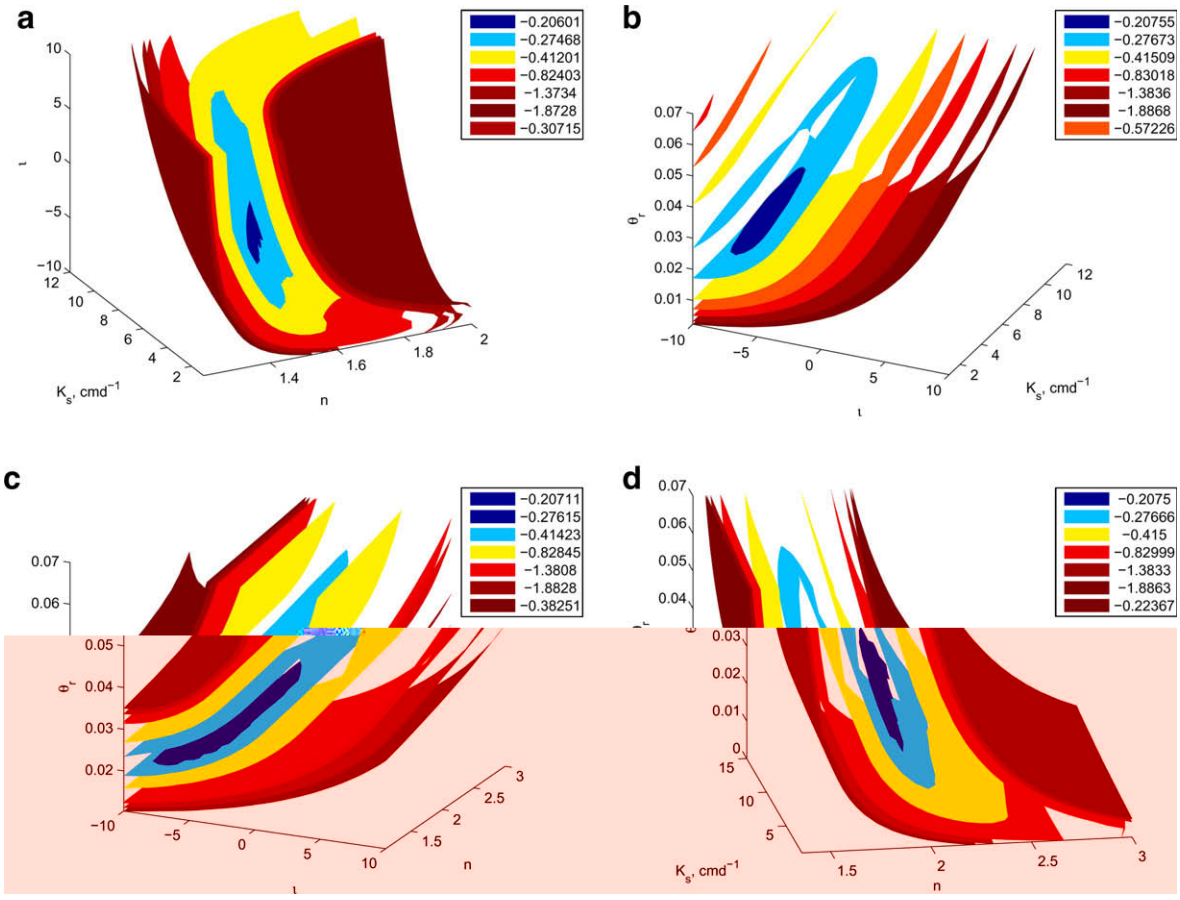

Fig. 9. Selected three-dimensional parameter hyper-space: $K_s - n_v - l$ (a), $l - K_s - \theta_r$ (b), $l - n_v - \theta_r$ (c), and $K_s - n_v - \theta_r$ (d) patches. The legend presents the logarithm of the penalty function at minimum.

The most accurate parameter estimation is obtained when the state variables have the highest sensitivities to the collected experimental data and to the model parameters being estimated [73]. Kinetic Monte Carlo and finite-difference-based methods as well as methods based on the Girsanov measure transformation have been extensively used to quantify the dependence of the system's behavior and dynamics on the parameters [68]. In this study, the sensitivity of the model with

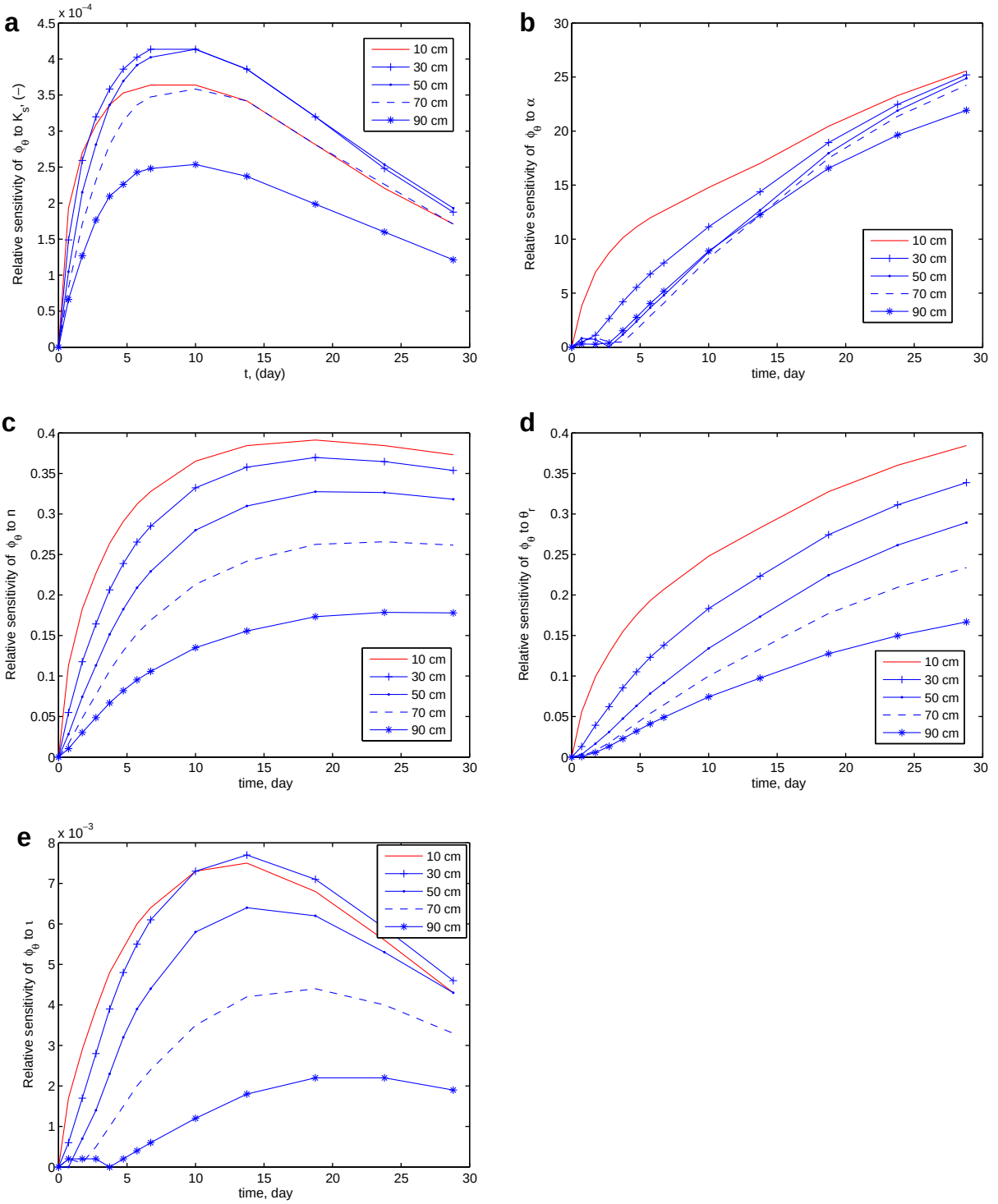

Fig. 10. The relative sensitivity of the penalty function with respect to the changes in different model parameters: (a) saturated hydraulic conductivity (K_s), (b) air entry value (α_v), (c) n_v, (d) residual soil moisture content (θ_r), and (e) pore connectivity index in Mualem's model (l) across space–time scales.

respect to changes in K_s, α_v, n_v, θ_r, and l was calculated by differentiation of Eq. (1) with respect to the parameter vector $p = [K_s \alpha_v n_v \theta_r l]$:

$$\frac{\partial}{\partial K_s}\left(\frac{\partial \theta}{\partial t}\right) = \frac{\partial}{\partial K_s}\left[\frac{\partial}{\partial z}K(h)\frac{\partial h}{\partial z}\right] - \frac{\partial}{\partial K_s}\left(\frac{\partial K}{\partial z}\right) \tag{31}$$

$$\frac{\partial}{\partial \alpha_v}\left(\frac{\partial \theta}{\partial t}\right) = \frac{\partial}{\partial \alpha_v}\left[\frac{\partial}{\partial z}K(h)\frac{\partial h}{\partial z}\right] - \frac{\partial}{\partial \alpha_v}\left(\frac{\partial K}{\partial z}\right) \tag{32}$$

$$\frac{\partial}{\partial n_v}\left(\frac{\partial \theta}{\partial t}\right) = \frac{\partial}{\partial n_v}\left[\frac{\partial}{\partial z}K(h)\frac{\partial h}{\partial z}\right] - \frac{\partial}{\partial n_v}\left(\frac{\partial K}{\partial z}\right) \tag{33}$$

$$\frac{\partial}{\partial \theta_r}\left(\frac{\partial \theta}{\partial t}\right) = \frac{\partial}{\partial \theta_r}\left[\frac{\partial}{\partial z}K(h)\frac{\partial h}{\partial z}\right] - \frac{\partial}{\partial \theta_r}\left(\frac{\partial K}{\partial z}\right) \tag{34}$$

$$\frac{\partial}{\partial l}\left(\frac{\partial \theta}{\partial t}\right) = \frac{\partial}{\partial l}\left[\frac{\partial}{\partial z}K(h)\frac{\partial h}{\partial z}\right] - \frac{\partial}{\partial l}\left(\frac{\partial K}{\partial z}\right) \tag{35}$$

Applying chain rule of differentiation to system (31)–(35) results in a system of five partial differential equations which were discretized and solved by a fully implicit backward in time (Euler time marching scheme) and central in space finite difference approximation. To compare the sensitivity of the model with respect to changes in different parameters the relative sensitivity, rather than the absolute sensitivity, was used. The sensitivities were calculated and compared across parameters, times, and locations to identify what should be measured where and when in the experiments in order to maximize the accuracy of the parameter estimation. The results are presented in Fig. 10. The soil depths in which measurements were made are given in the legend.

Fig. 10(a) indicates that the sensitivity of ϕ_θ with respect to the changes in K_s is high at the early stages of the drainage experiment. As drainage proceeds the sensitivity of ϕ_θ with respect to the changes in K_s decreases. The rate of decrease for the surface layer ($z = 10$ cm) is faster than for the subsurface layers. Therefore, to obtain reliable estimate for K_s more data should be collected at the beginning of the experiment or more weight should be given to the early data points in the parameter optimization algorithm.

Comparing Fig. 10(b) with other graphs and $\left\|\frac{\partial \theta}{\partial \alpha_v}\right\|$ with those of other parameters indicate that α_v is the most sensitive and identifiable parameter (see last column in Table 1). As drainage proceeds the sensitivity of the model with respect to the changes in α_v increases in all layers though the rate of change is high for surface layer. The same conclusion can be derived from 9c for n_v though the relative sensitivity of ϕ_θ with respect to the changes in n_v is less than $\alpha_v\left(\left\|\frac{\partial \theta}{\partial n_v}\right\| = 1.8203\right)$. As the soil becomes drier the sensitivity increases and stays almost constant over the time course of the drainage experiment. Note that the rate of increase is not as high as α_v and the sensitivity curves do not have a well-defined peak.

Sensitivity of ϕ_θ with respect to the changes in θ_r was plotted in Fig. 10(d). As drainage proceeds the sensitivity of ϕ_θ with respect to the changes in θ_r increases. The rate of increase in the surface layer ($z = 10$ cm) is greater than subsurface layers. The sensitivity does not have a well-defined peak implying that the residual soil water content should be well identified by the soil moisture data in very dry zone of the soil water characteristic curve.

The relative sensitivity of ϕ_θ with respect to the changes in pore connectivity index (l) is presented in Fig. 10(e). Although the sensitivity increases during time course of the drainage experiment (the increase is more pronounced for surface layer), the norm of the sensitivity vector is small ($\left\|\frac{\partial \theta}{\partial l}\right\| = 0.0316$). This may imply that the drainage experiment does not provide enough information to accurately estimate the pore connectivity index in Eq. (3). Multi-objective optimization or other kind of experimentation, such as infiltration, may produce informative space–time series to quantify this parameter. Note that the commonly used practice ($l = 0.5$) is a rough estimate and, therefore, is not recommended.

In conclusion, sensitivity analysis shows that α_v is the most identifiable parameter, by inverse modeling, followed by n_v and θ_r. The norms of the sensitivity vectors for these parameters are 8.4122, 1.8203, and 1.2739, respectively (see the last column in Table 1). The saturated hydraulic conductivity $\left(\left\|\frac{\partial \theta}{\partial K_s}\right\| = 0.0406\right)$ and pore connectivity index ($\left\|\frac{\partial \theta}{\partial l}\right\| = 0.0316$) are the least identifiable parameters among the hydraulic parameters.

6. Conclusion

An inverse modeling strategy was developed, implemented, and analyzed by coupling the Osborne–Moré modified form of the Levenberg–Marquardt algorithm with the Galerkin linear finite element solution of the mixed form Richards equation and in-situ soil moisture time–space series. To decrease CPU time and maintain acceptable truncation error, an adaptive time-stepping approach was used. The numerical simulator of the direct problem was mass-conservative and showed perfect agreement with a reference solution computed using a very small time step and dense grid in a test problem.

The inverse problem was treated as a nonlinear optimization problem in which model parameters were estimated by minimizing a penalty function representing the discrepancy between the measured and predicted soil moisture contents.

An adaptive algorithm was implemented to calculate the sensitivity matrix in the inverse algorithm. A multi-rule termination criterium was used to end the inverse code at the solution. The strategy was successfully used to determine hydraulic parameters of a partially saturated soil. The results of the optimization showed excellent agreement with the experimental data.

A novel sensitivity analysis was performed to analyze sensitivity of the model with respect to uncertainty and changes in different hydraulic parameters. Sensitivity analysis indicates that the *air entry value* (α_v) in van Genuchten's expression is the most identifiable parameter followed by n and the residual soil moisture content. The saturated hydraulic conductivity and pore connectivity index are the least identifiable parameters among the hydraulic parameters.

Analysis of the parameter response surfaces and three-dimensional hyper-space plots, closeness of the gradient of the objective function at minimum to zero, and positive definiteness of the approximation for the Hessian at the solution indicate that the obtained solution is a strong local minimum.

References

[1] M. Abramovitch, I.A. Stegun, Handbook of Mathematical Functions, Applied Math. Ser., fourth ed., vol. 55, US Government Printing Office, Washington DC, 1965.
[2] W.M. Alley, R.W. Healy, J.W. LaBaugh, T.E. Reilly, Flow and storage in groundwater systems, Science 296 (2002) 1985–1990.
[3] S. Assouline, D.M. Tartakovsky, Unsaturated hydraulic conductivity function based on a soil fragmentation process, Water Resour. Res. 37 (5) (2001) 1309–1312.
[4] S. Assouline, D. Tessier, A. Bruand, A conceptual model of the soil water retention curve, Water Resour. Res. 34 (1998) 223–231.
[5] Y. Bard, Nonlinear Parameter Estimation, Academic Press, New York, 1974.
[6] J.V. Beck, K.J. Arnold, Parameter Estimation in Science and Engineering, John Wiley, New York, 1977.
[7] R. Becker, B. Vexler, Mesh refinement and numerical sensitivity analysis for parameter calibration of partial differential equations, J. Comp. Phys. 206 (1) (2005) 95–110.
[8] H.M. Blackburn, S. Schmidt, Spectral element filtering techniques for large eddy simulation with dynamic estimation, J. Comp. Phys. 186 (2) (2003) 610–629.
[9] H. Bouwer, R.D. Jackson, Determining soil properties, in: J. van Schilfgaarde (Ed.), Drainage for Agriculture, ASA Monograph 17, Madison, WI, 1974.
[10] R.H. Brooks, A.T. Corey, Hydraulic properties of porous media, Technical Report Hydrology Paper No. 3, Colorado State University, Forth Collins, CO, 1964, 27 pp.
[11] E. Buckingham, Studies on the movement of soil moisture, Technical Report, USDA Bureau of Soils, Bulletin 38, 1907.
[12] N.T. Burdine, Relative permeability calculations from pore size distribution data, Petrol. Trans. Am. Inst. Min. Eng. 198 (1953) 71–77.
[13] R.F. Carsel, R.S. Parrish, Developing joint probability distributions of soil water characteristics, Water Resour. Res. 24 (1988) 755–769.
[14] M.A. Celia, E.T. Bouloutas, R.L. Zarba, A general mass conservative numerical solution for unsaturated flow equation, Water Resour. Res. 26 (1990) 1483–1496.
[15] G. Chavent, M. Dupuy, P. Lemonnier, History matching by using optimal theory, Soc. Petrol. Eng. J. 15 (1975) 74–86.
[16] J. Chen, J.W. Hopmans, M.E. Grismer, Parameter estimation of two-fluid capillary pressure–saturation and permeability functions, Adv. Water Resour. 22 (1999) 479–493.
[17] J. Crank, P. Nicolson, A practical method for numerical evaluation of solutions of partial differential equations of the heat conduction type, Proc. Camb. Philos. Soc. 43 (1947) 50–64.
[18] H. Darcy, Les Fontaines Publiques de la Ville de Dijon, in: M.K. Hubert (Ed.), The Theory of Groundwater and Related Papers, Hafner Pub. Co., New York, 1969.
[19] J.E. Dennis, J. Moré, Quasi-Newton methods: motivation and theory, SIAM Rev. 19 (1977) 46–89.
[20] H.J.G. Diersch, P. Perrochet, On the primary variable switching technique for simulating saturated–unsaturated flows, Adv. Water Resour. 23 (1999) 271–301.
[21] J.R. Donaldson, R.B. Schnabel, Computational experience with confidence regions and confidence intervals for nonlinear least squares, Technometrics 29 (1987) 67–82.
[22] T.O. Drews, R.D. Braatz, R.C. Alkire, Parameter sensitivity analysis of Monte Carlo simulations of copper electrodeposition with multiple additives, J. Electrochem. Soc. 150 (11) (2003) C807–C812.
[23] R.E. Ewing, T. Lin, A class of parameter optimization techniques for fluid flow in porous media, Adv. Water Resour. 14 (1991) 89–97.
[24] P.A. Forsyth, Y.S. Wu, K. Pruess, Robust numerical methods for saturated–unsaturated flow with dry initial conditions in heterogeneous media, Adv. Water Resour. 20 (1995) 1–14.
[25] G.H. Golub, C.F. van Loan, Matrix Computations, Johns Hopkins University Press, Baltimore, MD, 1983.
[26] R.E. Green, L.R. Ahuja, S.K. Chong, Hydraulic conductivity diffusivity and sorptivity of unsaturated soils: field method, in: A. Klute (Ed.), Methods of Soil Analysis, Part 1, ASA Monograph 9, Madison, WI, 1986.
[27] R. Gunawan, Y. Cao, L. Petzold, F.J. Doyle III, Sensitivity analysis of discrete stochastic systems, Biophys. J. 88 (4) (2005) 2530–2540.
[28] E.L. Haseltine, D.B. Patience, J.B. Rawlings, On the stochastic simulation of particulate systems, Chem. Eng. Sci. 60 (2005) 2627–2641.
[29] J. Helsing, Estimating effective properties of composites from cross-sectional photographs, J. Comp. Phys. 117 (2) (1995) 281–288.
[30] R.G. Hills, I. Porro, D.B. Hudson, P.J. Wierenga, Modeling one-dimensional infiltration into very dry soils, 1: model development and evaluation, Water Resour. Res. 25 (1989) 1259–1269.
[31] D.L. Hitzl, F.H. Maltz, Adaptive estimation procedures for multi-parameter Monte Carlo computations, J. Comp. Phys. 37 (2) (1980) 218–241.
[32] H.R. Hofmann, P.A. Hofmann, Darcy's law and structural explanation in hydrology, Proc. Biennial Meet. Philos. Sci. Assoc. 1 (1992) 23–35.
[33] P.S. Huyakorn, G.F. Pinder, Computational Methods in Subsurface Flow, Academic Press, San Diego, 1983.
[34] P.S. Huyakorn, S.D. Thomas, B.M. Thompson, Techniques for making finite element competitive in modeling flow in variably saturated media, Water Resour. Res. 20 (8) (1984) 1099–1115.
[35] S.I. Hwang, S.E. Powers, Estimating unique soil hydraulic properties for sandy media from multi-step outflow experiments, Adv. Water Resour. 26 (2002) 445–456.
[36] I. Javandel, P.A. Whiterspoon, Applications of the finite element method to transient flow in porous media, Soc. Petrol. Eng. J. 3 (1968) 241–252.
[37] M.R. Kirkland, R.G. Hills, P.J. Wierenga, Algorithms for solving Richards' equation for variably saturated soils, Water Resour. Res. 28 (1992) 2049–2058.
[38] I. Knowles, T. Le, A. Yan, On the recovery of multiple flow parameters from transient head data, J. Comput. Appl. Math. 169 (2004) 1–15.
[39] I. Knowles, A. Yan, On the recovery of transport parameters in groundwater modeling, J. Comput. Appl. Math. 171 (2004) 277–290.
[40] J.B. Kool, J.C. Parker, M.Th. van Genuchten, Parameter estimation for unsaturated flow and transport models – a review, J. Hydrol. 91 (1987) 255–293.
[41] K. Kosugi, Three-parameter lognormal distribution model for soil water retention, Water Resour. Res. 30 (4) (1994) 891–901.
[42] K. Kosugi, Lognormal distribution model for unsaturated soil hydraulic properties, Water Resour. Res. 32 (9) (1996) 2697–2703.
[43] M. Kowalsky, S. Finsterle, Y. Rubin, Estimating flow parameter distributions using ground-penetrating radar and hydrological measurements during transient flow in the vadose zone, Adv. Water Resour. 27 (2004) 583–599.

[44] L.K. Kuiper, A comparison of iterative methods as applied to the solution of nonlinear three-dimensional groundwater flow equation, SIAM J. Sci. Stat. Comput. 8 (4) (1987) 521–528.
[45] J. Lavergnat, J. Portes, M. Sylvain, A new algorithm to determine the parameters of a sinusoidal signal, J. Comp. Phys. 36 (3) (1980) 347–365.
[46] T. Lee, J.H. Seinfeld, Estimation of absolute and relative permeabilities in petroleum reservoirs, Inverse Probl. 3 (1987) 711–728.
[47] T. Lee, J.H. Seinfeld, Estimation of properties of two-phase petroleum reservoirs by regularization, J. Comp. Phys. 69 (1987) 397–417.
[48] D. Lesnic, L. Elliott, D.B. Ingham, Identification of the thermal conductivity and heat capacity in unsteady nonlinear heat conduction problems using the boundary element method, J. Comp. Phys. 126 (2) (1996) 410–420.
[49] K. Levenberg, A method for the solution of a certain non-linear problems in least squares, Q. Appl. Math. 2 (1944) 164–168.
[50] J.R. Macdonald, Comparison of parametric and nonparametric methods for the analysis and inversion of immittance data: critique of earlier work, J. Comp. Phys. 157 (1) (2000) 280–301.
[51] B. Malengier, Parameter identification in stationary groundwater flow problems in drainage basins, J. Comput. Appl. Math. 168 (2004) 299–307.
[52] D.W. Marquardt, An algorithm for least squares estimation of nonlinear parameters, SIAM J. Appl. Math. 11 (1963) 431–441.
[53] P.C.D. Milly, A mass conservative procedure for time stepping in models of unsaturated flow, Adv. Water Resour. 8 (1985) 32–36.
[54] J.J. Moré, The Levenberg–Marquardt algorithm: implementation and theory, in: G.A. Watson (Ed.), Numerical Analysis, Lecture Notes in Mathematics, vol. 630, Springer Verlag, 1978.
[55] Y. Mualem, A catalogue of the hydraulic properties of unsaturated soils, Technical Report 442, Israel Institute of Technology, Haifa, 1976.
[56] Y. Mualem, A new model for predicting hydraulic conductivity of unsaturated porous media, Water Resour. Res. 12 (1976) 513–522.
[57] S.P. Neuman, Galerkin approach to saturated–unsaturated flow in porous media, in: R.H. Gallagher et al. (Eds.), Finite Element in Fluids, vol. 1, John Wiley and Sons, New York, 1975.
[58] S.P. Neumann, J. Carrera, Maximum-likelihood adjoint-state finite-element estimation of groundwater parameters under steady and non-steady state conditions, J. Appl. Math. Comput. 17 (1985) 405–432.
[59] N.C. Nguyen, A posteriori error estimation and basis adaptivity for reduced-basis approximation of nonaffine-parametrized linear elliptic partial differential equations, J. Comp. Phys. 227 (2) (2008) 983–1006.
[60] N. Oreskes, K. Shrader-Frechette, K. Belitz, Verification, validation, and confirmation of numerical models in the earth science, Science 263 (1994) 641–646.
[61] M.R. Osborne, Nonlinear least squares-the Levenberg–Marquardt revisited, J. Aus. Math. Soc., Ser. B19 (1976) 343–357.
[62] L. Pan, P.J. Wierenga, A transformed head-based approach to solve Richards' equation for variably saturated soils, Water Resour. Res. 31 (1995) 925–931.
[63] L. Pan, P.J. Wierenga, A.W. Warrick, Finite element methods for modeling water flow in variably saturated porous media: Numerical oscillation and mass-distributed schemes, Water Resour. Res. 32 (1996) 1883–1889.
[64] L. Pan, L. Wu, A hybrid global optimization method for inverse estimation of hydraulic parameters: annealing-simplex method, Water Resour. Res. 34 (1998) 2261–2269.
[65] C. Paniconi, A.A. Aldama, E.F. Wood, Numerical evaluation of iterative and noniterative methods for the solution of the nonlinear Richards' equation, Water Resour. Res. 27 (6) (1991) 1147–1163.
[66] C. Paniconi, M. Putti, A comparison of Picard and Newton iteration in the numerical solution of multidimensional variably saturated flow problems, Water Resour. Res. 30 (12) (1994) 3357–3374.
[67] G.F. Pinder, W.G. Gray, Finite Element Simulation in Surface and Subsurface Hydrology, Academic Press, New York, 1977.
[68] S. Plyasunov, A.P. Arkin, Efficient stochastic sensitivity analysis of discrete event systems, J. Comp. Phys. 221 (2007) 724–738.
[69] S. Raimondeau, P. Aghalayam, A.B. Mhadeshwar, D.G. Vlachos, Parameter optimization in molecular models: application to surface kinetics, Ind. Eng. Chem. Res. 42 (2003) 1174–1183.
[70] L.A. Richards, Capillary conduction of liquids in porous media, Physics 1 (1931) 318–333.
[71] D. Russo, E. Bresler, U. Shani, J.C. Parker, Analyses of infiltration events in relation to determining soil hydraulic properties by inverse modeling methodology, Water Resour. Res. 27 (1991) 1361–1373.
[72] K. Sadegh Zadeh, Multi-scale inverse modeling in biological mass transport processes, Ph.D. Thesis, Fischell Department of Bioengineering, University of Maryland at College Park, 2006.
[73] K. Sadegh Zadeh, Multi-objective optimization in variably saturated fluid flow, J. Comput. Appl. Math. (2008), doi:10.1016/j.cam.2008.03.005.
[74] K. Sadegh Zadeh, H.C. Elman, H.J. Montas, A. Shirmohammadi, A finite element model for protein transport in vivo, BioMed. Eng. Online, 6:24, doi:10.1186/1475-925X-6-24, 2007.
[75] K. Sadegh Zadeh, H.J. Montas, A. Shirmohammadi, A mass conservative algorithm for simulating saturated–unsaturated flow in porous media, in: AS ABE Annual International Meeting, Paper 063053, July 9–14, Portland, OR, 2006.
[76] K. Sadegh Zadeh, H.J. Montas, A. Shirmohammadi, Identification of biomolecule mass transport and binding rate parameters in living cells by inverse modeling, Theor. Biol. Med. Mod. 3 (2006) 36, doi:10.1186/1742-4682-3-36.
[77] K. Sadegh Zadeh, A. Shirmohammadi, H.J. Montas, G. Felton, Evaluation of infiltration models in contaminated landscape, J. Environ. Sci. Health A Tox. Hazard. Subst. Environ. Eng. 42 (7) (2007) 983–988.
[78] G.A.F. Seber, C.J. Wild, Nonlinear Regression, John Wiley and Sons, New York, 2004.
[79] L.J. Segerlind, Applied Finite Element Analysis, John Wiley and Sons, New York, 1984.
[80] J. Šimunek, M.Th. van Genuchten, Estimating unsaturated soil hydraulic properties from tension disc infiltrometer data by numerical inversion, Water Resour. Res. 32 (1996) 2683–2696.
[81] N.-Z. Sun, Inverse Problem in Groundwater Modeling, Kluwer Academic Publishers, Dordrecht, The Netherlands, 1994.
[82] M.D. Tocci, C.T. Kelly, Accurate and economical solution of the pressure-head form of Richards' equation by the method of lines, Adv. Water Resour. 20 (1) (1997) 1–14.
[83] K. van den Doel, U.M. Ascher, On level set regularization for highly ill-posed distributed parameter estimation problems, J. Comp. Phys. 216 (2) (2006) 707–723.
[84] M.Th. van Genuchten, Numerical solutions of the one-dimensional saturated–unsaturated flow equation, Technical Report 78-WR-9, Water Resources Program, Department of Civil Engineering Princeton University, NJ, 1978.
[85] M.Th. van Genuchten, A comparison of numerical solutions of the one-dimensional unsaturated flow and mass transport equations, Adv. Water Resour. 5 (1982) 47–55.
[86] M.Th. van Genuchten, F.J. Leij, S.R. Yates, The RETC code for quantifying the hydraulic functions of unsaturated soils, Technical Report, EPA/600/S2-91/065, USEPA, Robert S. Kerr Environmental Research Laboratory, Ada, OK, 1991.
[87] W.G. Yeh, Review of parameter estimation procedures in groundwater hydrology: the inverse problem, Water Resour. Res. 22 (1986) 95–108.
[88] D.E. Zak, G.E. Gonye, J.S. Schwaber, F.J. Doyle III, Importance of input perturbations and stochastic gene expression in the reverse engineering of genetic regulatory networks: insights from an identifiability analysis of an in silico network, Genome Res. 13 (2003) 2396–2405.
[89] C. Zheng, G.D. Bennett, Applied Contaminant Transport Modeling, John Wiley and Sons, New York, 2002.
[90] O.C. Zienkiewicz, Finite Element Methods in Structural and Continuum Mechanics, McGraw-Hill, London, 1967.